Entamoeba histolytica EHD1 is involved in mitosome-endosome contact

Herbert J. Santos[a,b] , Yuki Hanadate[b], Kenichiro Imai[c], Haruo Watanabe[d], and Tomoyoshi Nozaki[a,b*]

[a]Department of Biomedical Chemistry, Graduate School of Medicine, The University of Tokyo, 7-3-1 Hongo, Bunkyo-ku, Tokyo 113-0033, Japan;

[b]Department of Parasitology, National Institute of Infectious Diseases, 1-23-1 Toyama, Shinjuku-ku, Tokyo 162-8640, Japan;

[c]Cellular and Molecular Biotechnology Research Institute, National Institute of Advanced Industrial Science and Technology (AIST), 2-4-7 Aomi, Koto-ku, Tokyo 135-0064, Japan;

[d]Department of Bacteriology, National Institute of Infectious Diseases, 1-23-1 Toyama, Shinjuku, Tokyo 162-8640, Japan

* Correspondence: nozaki@m.u-tokyo.ac.jp

Abstract

Inter-organellar crosstalk is often mediated by membrane contact sites (MCSs), which are zones where participating membranes come within a proximity of 30 nm. MCSs have been found in organelles including the endoplasmic reticulum, Golgi bodies, endosomes, and mitochondria. Despite its seeming ubiquity, reports of MCS involving mitochondrion-related organelles (MROs) present in a few anaerobic parasitic protozoa remain lacking. Entamoeba histolytica, the etiological agent of amoebiasis, possesses an MRO called mitosome. We previously discovered several Entamoeba-specific transmembrane mitosomal proteins (ETMPs) from in silico and cell biological analyses.

One of them, ETMP1 (EHI_175060), was predicted to have one transmembrane domain and two coiled-coil regions, and was demonstrated to be mitosome membrane-integrated based on carbonate fractionation and immunoelectron microscopy (IEM) data. Immunoprecipitation analysis detected a candidate interacting partner, EH-domain containing protein (EHD1, EHI_105270). We expressed HA-tagged EHD1 in E. histolytica and subsequent immunofluorescence and IEM data indicated an unprecedented MCS between the mitosome and the endosome. Live imaging of GFP-EHD1 expressing strain demonstrated that EHD1 is involved in early endosome formation, and is observed in MCS between endosomes of various sizes. In vitro assay using recombinant His-EHD1 demonstrated ATPase activity. MCSs are involved in lipid transfer, ion homeostasis, and organelle dynamics. The serendipitous discovery of the ETMP1 interacting partner EHD1, led to the observation of the mitosome-endosome contact site in E. histolytica. It opened a new view of how the relic mitochondria of Entamoeba may likewise be involved in organelle crosstalk, a conserved feature of mitochondria and other organelles in general.

Abstract word count: 248 words

Introduction

Membrane contact sites (MCSs) mediate communication and exchanges between membrane-bound compartments by the assembly of protein-protein or protein-lipid tethers which maintains distancing of 30 nm between interacting membranes. MCSs have been found in almost every pair of organelles (1), most of which involving the endoplasmic reticulum (ER) as its membrane spans a network that interacts with the plasma

membrane, and other organellar membranes such as those of the Golgi apparatus, lysosomes, endosomes, lipid droplets, peroxisomes, and mitochondria (2). MCSs are also reported between other organelle pairs such including the peroxisomes and lipid droplets, and the mitochondria and vacuoles/endosomes/lysosomes, plasma membrane, lipid droplets, and peroxisomes respectively, notwithstanding the contact sites between the inner and outer mitochondrial membranes (3). These contact sites mostly harbor proteins involved in lipid metabolism and transport, making them hubs of lipid transfer between interacting membranes. However, other processes associated with MCSs have been reported and they include ion transport and homeostasis, apoptosis (1), and endosomal (4) and mitochondrial (5) fission, respectively.

We recently identified several key molecules that facilitate membrane contact sites in mitosomes, endosomes, and Golgi apparatus of *Entamoeba histolytica*, and aimed to study their roles and possible link to the parasitic nature of this amoeba. *E. histolytica* is an anaerobic unicellular protozoan parasite that infects the large intestine of humans, and causes amebiasis, a disease characterized by diarrhea, which is a major cause of death in children worldwide. Millions of individuals are infected; mostly in developing countries and the disease causes an estimated 100,000 deaths annually (6). Infection begins by the ingestion of infectious cysts, which are resistant to the acidic environment of the stomach, then cysts pass through the small intestine, and undergo excystation within the terminal ileum or colon, to the trophozoite stage. Trophozoites reproduce and encyst within the colon, where they are released in the environment via excretion of feces, thus completing one cycle of the fecal-oral transmission (Stanley, 2003). Invasive amoebic trophozoites destroy the muco-epithelial barrier of the host intestinal tract, inducing mucus

overproduction, inflammation and dysentery. It could lead to the formation of extra-intestinal abscesses particularly in the liver (amoebic liver abscess), lungs, and brain. The virulence of this parasite is due to its ability to inflict damage to host cells and tissues, via parasite attachment to colonic epithelial cells, protease secretion to damage host cells and evade host immune response, and by ingestion of host cells via phagocytosis and trogocytosis. These processes involve intracellular trafficking and inter-organellar crosstalk, underscoring the role of vesicular transport and membrane contact sites (MCSs) not only in parasite biology but also in its virulence and pathogenesis.

Like other anaerobic parasitic protozoans, *E. histolytica* lacks canonical mitochondria, and instead has a highly divergent mitochondrion-related organelle (MRO) called mitosome. *Entamoeba* mitosomes contribute to parasitism (7) due to a compartmentalized sulfate activation pathway that leads to the formation of cholesteryl sulfate in the cytosol. This molecule induces stage conversion from the trophozoite to cyst form (8) a process that is essential for maintaining the parasite's life cycle and mode of disease transmission. Apart from mitosomes, other amoebic organelles such as the ER and the Golgi apparatus also show less defined structural and compositional features compared with model organisms, however, they have been shown to contain orthologs of established endomembrane proteins (9–11). Our knowledge on MCSs in *Entamoeba* is extremely limited, with only the previously identified mitosomal membrane proteins ETMP30 (reported to interact with a Golgi-localized protein secretory pathway calcium ATPase) and EHI_099350 (reported to have dual localization in the mitosomes and the ER) (12–14). Other molecules that participate in tethering of these compartments and what roles these contact sites play in the cell are still unknown, making it imperative to

dissect amoebic MCSs. These past observations point to the fact that mitosomes, although highly degenerate, are able to interact with other organelles in the cytoplasm, and such contacts often utilize lineage-specific membrane. Here we identified another mitosomal membrane protein, ETMP1 which interacts with a C-terminal Eps15 homology domain (EHD) containing protein, a member of the EHD protein superfamily involved in various endocytic processes. Studies on *E. histolytica* organelle interaction via the endocytic transport mechanism has accumulated over several decades, including proteins involved in cargo sorting regulation and endosome dynamics such as Rab GTPases (15) and endosomal sorting complex required for transport (ESCRT) proteins (16, 17). However, there are so far no reports on whether these molecules take part in MCS between endosomes and other parts of the cell.

Results

EHI_175060 is a lineage-specific mitosomal membrane protein

Our group previously searched for transmembrane domain-containing mitosomal proteins using a previously-developed prediction pipeline (12) in sought for proteins that could be lineage-specific receptors, channels, enzymes, and components of the import machinery or otherwise uncharacterized complexes on the outer and inner membranes of *Entamoeba histolytica* mitosomes. This resulted in the prediction of 25 protein candidates. Like the other 24 proteins in the list (12), EHI_175060 is unique to the lineage *Entamoeba*. Figure 1 shows a multiple sequence alignment of the protein sequence of EHI_175060 with that of its orthologs in other *Entamoeba* species (*E. moshkovskii*, *E. dispar*, and *E. nuttalli*). The protein has a predicted molecular mass of 29.5 kDa, and it

contains two coiled-coil domains at the middle portion and a single transmembrane domain near the carboxyl terminus. It also lacks a predictable canonical N-terminal targeting sequence. Based on these characteristics, we name EHI_175060, as *Entamoeba*-specific transmembrane mitosomal protein 1 (ETMP1).

ETMP1 is localized to mitosomal membranes

To validate the predicted localization of ETMP1, we expressed amino terminus hemagglutinin (HA)-tagged fusion protein, HA-ETMP1, in amoebic trophozoites and confirmed protein expression by Western blot analysis. The anti-HA immunoblot showed a single band corresponding to the expected molecular mass of HA-ETMP1 (Figure 2A). We then analyzed the localization of the protein by immunofluorescence assay (IFA; Figure 2B). Co-staining of HA-ETMP1 expressing strain using anti-HA antibody and anti-adenosine-5'-phosphosulfate kinase (APSK; EHI_179080; a mitosomal matrix enzyme involved in sulfate activation) antiserum revealed good colocalization of the HA-tagged protein to mitosomes containing APSK. This is supported by the Pearson correlation R value which ranges between 0.31 to 0.59, suggesting that HA-ETMP1 is localized to mitosomes. Furthermore, we also performed Percoll-gradient fractionation of HA-ETMP1 homogenate and found that fractions containing HA-ETMP1 showed broad distribution in the first ultracentrifugation, suggesting some proteins are localized to the cytosol/lighter fractions. However, HA-ETMP1 also exists in the bottom fractions which overlap with those that contain chaperonin 60 (Cpn60; EHI_178570; a chaperone protein and canonical mitochondrial matrix marker). The co-fractionation of HA-ETMP1 to mitosomes was suggested by the anti-HA and anti-Cpn60 immunoblots of both the first and second ultracentrifugation respectively (Figure 2C). We also performed subcellular fractionation

followed by carbonate treatment, to further assess the localization, as well as membrane integration of HA-ETMP1. The fractionation profile of HA-ETMP1 after immunoblot analysis (Figure 2D, upper panel) showed that it is present in both cytosolic and organelle fractions. Also, it was clearly demonstrated that the HA-ETMP1 contained in the organellar membrane-enriched fraction, is integrated to organellar membranes as it was retained in the particulate fraction after carbonate treatment, similar to MBOMP30-HA (Figure 2D, middle panel), a positive control for mitosomal membrane protein. These carbonate fractionation profiles contrast with that of the soluble mitosomal matrix protein marker Cpn60, as shown by the blot stained with anti-Cpn60 antiserum (Figure 2D, bottom panel).

We also performed immunoelectron microscopy analysis, and the results indicated that HA-ETMP1 is localized to the mitosome membranes, as anti-HA gold particles are found along the periphery of the Cpn60-labeled mitosomes (Figure 2E). Particle distribution analysis of the gold-conjugated antibodies revealed a significant difference in the staining of mitosomes (368 ± 279/ μm^2) compared to cytosol (22.3 ± 9.25/ μm^2) by anti-HA gold. The distribution of the mitosomal marker APSK as detected by the gold anti-APSK particles was also significantly higher in mitosomes (192 ± 98.1/ μm^2) than in the cytosol (0.984 ± 0.817/ μm^2). Statistical significance in both datasets was analyzed using two-tailed Welch's unequal variance t-test (n = 17, $p < 0.0001$). Overall, these data provide evidence of mitosomal membrane localization of ETMP1.

ETMP1 is essential and its overexpression causes drastic growth defect

We made several attempts at silencing the *etmp1* gene by small-RNA transcriptional interference, all of which failed as the transformants did not survive drug

selection, suggesting its essentiality to the parasite. We also observed a slower growth rate in HA-ETMP1 expressors compared with mock control. Analysis of growth kinetics of the two strains at varying concentrations of geneticin (G418) suggest a dose-dependent effect of drug concentration to the growth of amebic trophozoites (Figure 3A), and protein expression respectively (Figure 3B).

ETMP1 interacts with EH-domain containing proteins

To shed light on the function of ETMP1, we next attempted to identify its interacting partner(s) by immunoprecipitation (IP). Anti-HA agarose beads were used to immunoprecipitate the bait protein together with its binding partner(s) from the organelle-rich fraction of HA-ETMP1-expressing and mock control strains respectively. Western blotting with anti-HA antibody confirmed successful binding to and elution from HA-ETMP1 with respect to the anti-HA beads (Figure 4A). Silver staining of the SDS-PAGE gel containing HA peptide-eluted fractions revealed a band corresponding to approximately 55 kDa that is uniquely precipitated in HA-ETMP1 (absent in the mock-HA control) (Figure 4B). Protein sequencing analysis by mass spectrometry followed by differential comparison of quantitative values (QVs), normalized with unweighted spectrum counts between HA-ETMP1 and mock-HA control identified interacting partners of ETMP1 (Figure 4C). A cutoff of QV >2.0 in the HA-ETMP1 over the mock-HA sample was used, yielded four candidates, three of which were exclusively detected in the eluted IP fraction of HA-ETMP1. Also, three of the four candidates were identified in the mitosome proteome that was previously published (18), namely, L-myo-inositol-1-phosphate synthase (EHI_070720), EH-domain (EHD) containing protein 1 (annotated as

184 receptor mediated endocytosis protein; EHI_105270) and its close homolog, EHD2
185 (EHI_152680).

186 We also performed Blue Native (BN)-PAGE analysis to assess whether ETMP1 is
187 part of a protein complex. Anti-HA immunoblot analysis of BN-PAGE run samples
188 indicated that HA-ETMP1 forms complexes of about 90 kDa and 180 kDa respectively
189 (Figure 4D). Protein sequencing analysis of the excised silver-stained BN-PAGE bands
190 containing these two complexes identified numerous proteins. Similarly, we set a cutoff
191 value of >2.0 and the list of proteins are found in Supplementary Table S1A-C. Notably,
192 EHD1 and its close homolog EHD3 (97% identical) were identified in both the 90 and 180
193 kDa complex bands. Thus, we regarded EHD1 as one of the potential interacting partners
194 of ETMP1.

195 ***EHD1 is an ETMP1-interacting protein that is localized to mitosomes and to***
196 ***vesicles of varying sizes***

197 We expressed EHD1 in amoeba trophozoites with HA-tag at the amino terminus,
198 as confirmed by the anti-HA immunoblot result showing a band corresponding to the
199 expected molecular mass of HA-EHD1 (~61 kDa) (Figure 5A). To analyze and confirm
200 the mitosomal localization of EHD1, we performed double-staining IFA on HA-EHD1
201 expressing strain with anti-HA antibody and anti-APSK antiserum. We observed that the
202 anti-HA signal is mostly localized to the membrane of vesicles of various sizes (Figure
203 5B). We could also notice a few punctate anti-HA signals which colocalized with the anti-
204 APSK mitosome marker (Figure 5C, white arrowheads). Although minimal colocalization
205 between anti-HA and anti-APSK signals were observed, some anti-APSK signals were
206 notably seen near the vesicle membranes marked with HA-EHD1 (Figure 5C, white

arrow). Immunoelectron analysis (Figure 5D) corroborate the IFA observations, as we observed mostly vesicular membrane staining of anti-HA gold particles (left panel), with occasional signals on mitosomal membranes (middle panel), some of which showed close proximity to vesicular membranes (right panel). Furthermore, immunoblot analysis of Percoll-gradient fractions indicated wide distribution of HA-EHD1 across various densities, mostly in fractions 9 to 10 and with weaker intensity in fractions 12 to 22 of the first ultracentrifugation, and in fractions A to N in the second ultracentrifugation (Figure 5E), validating the microscopic observations of HA-EHD1 vesicular and mitosomal localization.

As majority of the signals of HA-EHD1 appear on vesicles, we next characterized the vesicles marked by HA-EHD1 by performing co-staining IFA using anti-HA antibody and one of the following antisera respectively: anti-vacuolar protein sorting 26 (Vps26), anti-pyridine nucleotide transhydrogenase (PNT), and anti-Rab11B. Most of the anti-HA-stained vesicles were colocalized with anti-Vps26- rather than anti-PNT- and anti-Rab11B-stained vesicles (Figure 6A) as supported by the Pearson correlation R value ranges of 0.22 to 0.37 for anti-Vps26, -0.16 to 0.19 for anti-PNT and 0.12 to 0.01 for anti-Rab11B, respectively. Vps26 is a retromer complex component and is a marker of endosomes/phagosomes in *E. histolytica* (19, 20). PNT is localized to the membrane of numerous vesicles/vacuoles, including lysosomes and phagosomes (21), while Rab11B was demonstrated to partially colocalize with late endosomes (22). Together, these data suggest EHD1 is mostly localized to endosomal membranes which may contain Vps26 and to some extent PNT, but not Rab11B.

HA-EHD1 is weakly associated to organellar membranes and preferentially binds to PI(3,5)P_2 and PI(4,5)P_2

We performed a similar carbonate fractionation assay to the organelle-enriched fraction of HA-EHD1 expressing strain. Based on the anti-HA immunoblots, HA-EHD1 was exclusively contained in the organelle fraction, as compared to that of the anti-CS1 profile which represents cytosolic fraction (Figure 6B). Next, we also assessed membrane integration of HA-EHD1 by carbonate treatment of the organelle-enriched fraction. Results of the immunoblots showed that HA-EHD1 is not membrane-bound as compared to the lysosomal membrane protein marker CPBF1 (Figure 6B). Instead, the profile is similar to that of the blot immunostained with an antiserum targeting Sec13, a peripheral ER membrane protein (Figure 6B). This suggests that HA-EHD1 is not organellar membrane-integrated, rather is weakly organellar membrane-associated.

To validate and characterize the phospholipid binding capacity of EHD1, we carried out a lipid overlay assay using lysates of HA-EHD1 and HA-SNX1 (PI3P binding protein control) respectively. Results indicated preferential binding of HA-EHD1 to phosphoinositide diphosphates, specifically PI(3,5)P2 and PI(4,5)P2 (Figure 6C).

Overexpression of HA-EHD1 demonstrated enhanced multivesicular body (MVB) formation

We also expressed HA-EHD1 under the control of tetracycline (tet) induction. IFA analysis of HA-EHD1 showed the protein is similarly localized to membranes of various vesicles after 1 h and 3 h of tet induced expression respectively (Figure 7A upper and middle panel). However, at 24 h post induction with tet, we noticed drastic changes in the localization as well as in the overall intracellular vesicular patterns of expressing

trophozoites (Figure 7A bottom panel), wherein large multivesicular bodies (MVBs) that were also marked with anti-HA signal were observed (Supplementary Movie S1). These findings were also supported by immunoelectron micrographs, showing immunodecoration of gold anti-HA particles along the membranes of MVBs, including the neck of invaginated vesicles (Figure 7B), after 24 h of tet-induced expression of HA-EHD1. These data point to the involvement of EHD1 in the biogenesis of MVBs in *E. histolytica*.

EHD1 is involved in early endosome formation during macropinocytosis and receptor-mediated endocytosis

To further characterize the vesicles whose membranes are associated with EHD1, we performed endocytosis assay using either dextran conjugated to rhodamine B isothiocyanate (RITC) (for bulk endocytosis and macropinocytosis) as well as transferrin conjugated to Alexa Fluor-568 (for receptor-mediated endocytosis) respectively, as substrates, which were chased by live (GFP-EHD1 and mock-GFP) or fixed (HA-EHD1 and mock-HA) imaging analysis of treated strains. Expression of GFP-EHD1 was confirmed as a single band after anti-GFP immunoblotting (Figure 8A). From imaging of live GFP-EHD1, we observed that the GFP signals are evenly spread on round endosomal membranes (Figure 8B left panel). However, signal polarization occurs on portions where there is contact between two endosomes (Supplementary Movie S2). We also observed localization of GFP-EHD1 in endosomes that contain either RITC-dextran and Alexa Fluor 568-transferrin (Figure 8B middle and right panels respectively). Our observations also revealed that EHD1 is involved in early endosome formation during macropinocytosis of RITC-dextran. Membranes of newly formed vesicles after ingestion of RITC-dextran initially did not contain EHD1 but several seconds later, GFP-EHD1

showed intense signal on the membrane of the enclosing early endosome (Supplementary Movie S3). Consistent with this, we also noticed a similar phenomenon of GFP-EHD1 recruitment in closing early endosomes when Alexa Fluor-568-transferrin was used as substrate (Supplementary Movie S4). In addition, we observed accumulation of transferrin on to certain spots in the plasma membrane which showed remarkably high GFP-EHD1 signal (Supplementary Movie S5). This suggests that EHD1 is also involved in intra-vesicular traffic of transferrin with some aggregate signals localized near the PM, likely hinting at its involvement in receptor or membrane recycling.

HA-EHD1 is localized to phagosome and trogosome membrane

To further characterize EHD1-containing vesicles, we performed phagocytosis assay by co-incubating expressing trophozoites with CellTracker Blue-stained Chinese hamster ovary (CHO) cells. Live and fixed-cell imaging analyses of phagosomes or trogosomes containing whole, or bites of CHO cells, respectively were observed at varying time points after co-incubation. We observed association of either GFP-EHD1 or HA-EHD1 on some phagosome and trogosome membranes (Figure 9). We also noticed patches of higher intensity signals on certain regions of contact between phago- or trogosomes and other vesicles in both fixed (Supplementary Movie S6) and live (Supplementary Movie S7) cell imaging analyses. IFA images also suggest that HA-EHD1 is localized at the phagocytic cup/tunnel suggesting its involvement in early phagosome formation (Figure 9 top panel; 15 min post coincubation). Also observed in fixed cells was the localization of HA-EHD1 on the trogosome membrane that appears to undergo tubulation (Figure 9, bottom panel; 60 min post co-incubation).

Recombinant His-EHD1 demonstrated ATPase activity in vitro

298 We also expressed amino terminus histidine (His)-tagged *E. histolytica* EHD1 in
299 bacteria to assess its enzymatic activity in vitro. We purified His-EHD1 using nickel-
300 nitriloacetic acid (Ni-NTA)-agarose beads as shown by the Coomassie Brilliant Blue-
301 stained SDS-PAGE gel, as well as the anti-His antibody-stained PVDF membrane (Figure
302 10A), containing representative Ni-NTA purification fractions. Eluted fraction of purified
303 His-EHD1 demonstrated ATPase activity (Figure 10B) with a Michaelis-Menten constant
304 (Km) value of 94.91 ± 16.63 μM and a maximum velocity (V_{max}) of 9.85 ± 0.37
305 μmole/min/mg.
306
307 **Discussion**
308 We have verified our prediction of ETMP1 being localized to the mitosomal
309 membrane by imaging and fractionation analyses. The gene encoding for this protein is
310 essential to the parasite's proliferation as indicated by the failure of transfected
311 trophozoites to survive sublethal concentration of drug pressure, compared with those
312 transfected with an empty vector control. Previous attempts at silencing the genes
313 encoding other mitosomal membrane proteins such as Tom40 (23) and MBOMP30 (24)
314 also failed, suggesting the essential role that these proteins, and the mitosome itself
315 where they exclusively localize, maintain in the proliferation of *E. histolytica*.
316 Overexpression of ETMP1 also affected the growth rate of the parasite negatively. This
317 may be due to the disruption of tight regulatory mechanisms for maintaining mitosomal
318 homeostasis and/or formation of toxic protein aggregates. It could also be due to the
319 stoichiometric imbalance of HA-ETMP1-containing protein complexes. Our BN-PAGE
320 analysis identified ETMP1 in the 90kDa and 180 kDa complexes respectively, whose

formation, compositional ratios, and biological functions may be sensitive to ETMP1 overexpression.

HA-ETMP1 immunoprecipitated a unique ~55 kDa protein. Mass spectrometry analysis of the excised silver-stained gel band indicated several candidates including EH-domain containing protein (EHD1; EHI_105270; 58 kDa) and its ortholog (EHD2; EHI_152680; 58 kDa) sharing 82% identity, vacuolar protein sorting-associated protein 45 (60 kDa; EHI_154290), and L-myo-inositol-1-phosphate synthase (57 kDa; EHI_070720). Incidentally, when we sequenced the complex band of 90 and 180 kDa BN-PAGE complex bands that include HA-ETMP1, we identified EHD1 and its close homolog EHD3 (EHI_052870; 58 kDa) with 97% identity. From these data, we deduced a plausible interaction between ETMP1 and EH domain containing proteins, with a focus on EHD1 in this paper. Repeated multiple attempts at immunoprecipitating the said complexes failed. One possibility is that the topology of HA-ETMP1 in the complex blocked the HA epitope tag from binding to the anti-HA beads. We also performed IP using HA-EHD1 (Supplementary Figure S1, Supplementary Table S2A), however our protein sequencing analysis of the ~30-37 kDa excised band did not detect HA-ETMP1 (Supplementary Table S2B), suggesting the likely transient nature of this protein binding. The detection of amoebic EHD isotypes in the pull-down and BN-PAGE complexes of HA-ETMP1 respectively, suggests potential interaction among these EHD homologs. It is also plausible that amoebic EHDs form hetero-dimers or hetero-oligomers as was demonstrated by mouse EHD1 and EHD3. The interaction between mouse EHD1 and EHD3 is likely involved in the regulation of recycling endosomes movement along microtubules (25). In *E. histolytica,* such EHD oligomers may be involved not only during

endocytosis but may also exist during the formation and maintenance of the mitosome-endosome contact. Compositional variations of EHD homo- or hetero-oligomers may also exist, and their corresponding functions may be stoichiometry-dependent.

EHDs have been associated to play roles in various endocytic processes. In one subset known as the C-terminal EHDs, four paralogues are present in mammals, namely EHD1, EHD2, EHD3, and EHD4. Mammalian EHD1 regulates exit of proteins from the endocytic recycling compartment to the plasma membrane, while both EHD1 and EHD3 have similar roles in controlling early endosome to Golgi transport (26, 27). Mammalian EHD2 localizes to caveolae and together with the Bin Amphiphysin Rvs (BAR)-domain containing binding partner PACSIN2, stabilizes caveolae at the cell surface (28), whereas mammalian EHD4 facilitates macroendocytic uptake of tropomyosin receptor kinase (Trk) receptors (29). EHDs are also implicated in the regulation of endocytic pathways associated with lipid metabolism. Mammalian EHD1 is involved in cholesterol homeostasis, affecting generation of cholesterol and triglyceride lipid bodies (30).

EHDs also regulate endocytosis in other organisms including plants, worms, and protozoans. *Arabidopsis thaliana* has two EHD paralogs, *At*EHD1 and *At*EHD2. Downregulation of *At*EHD1 led to a deficiency in the entry of endocytosed material into plant cells, whereas overexpression of *At*EHD2 caused an inhibitory effect on endocytosis, suggesting both proteins are important components in plant endocytic machinery (31). The EHD ortholog in *Caenorhabditis elegans*, receptor-mediated endocytosis 1 (Rme1), localizes to the endocytic recycling compartment and mediates the exit of cargo proteins to the cell membrane (32). In the protozoan parasite that causes malaria, *Plasmodium falciparum,* a single EHD protein is encoded in its genome. *Pf*EHD is involved in

367 endocytosis and plays a role in the generation of endocytic vesicles at the plasma
368 membrane, that are subsequently targeted to the neutral lipid generation/storage site
369 localized near the food vacuole (33). In the free-living amoebozoan *Dictyostelium*
370 *discoideum*, a single gene encoding EHD protein was identified. *Dd*EHD was determined
371 to be involved in phagosome maturation, and its deletion resulted to defects in
372 intraphagosomal proteolysis and acidification, early delivery of lysosomal enzymes, and
373 fast retrieval of the vacuolar H^+-ATPase in maturing phagosomes (34).

374 We have shown that *Eh*EHD1 is involved in various endocytic processes. Our live
375 imaging analysis showed involvement of *Eh*EHD1 in early endosome formation,
376 particularly during closure of newly-formed endosomes after engulfment of either RITC-
377 dextran (Supplementary Movie S3) or Alex568-transferrin (Supplementary Movie S4),
378 suggesting that *Eh*EHD1 may participate in the scission of early endosomes generated
379 from macropinocytosis as well as receptor-mediated endocytosis. Vesicle tubulation and
380 scission are associated roles of EHDs as they possess a dynamin-like ATPase domain
381 as demonstrated previously in (34–37).

382 Our in vitro enzyme assay showed that His-EHD1 has ATPase activity with a Km
383 value of 94.91 ± 16.63 μM as compared to the previously reported Km values for mouse
384 EHD1 (80 μM) and *Ce*RME1 (30-μM) (38). We also attempted to investigate the role of
385 ATPase activity of EHD1 in *E. histolytica* by expressing ATPase-deficient dominant
386 negative mutant, however the transfectants did not survive drug selection, suggesting the
387 importance of EHD1 ATP hydrolysis in amoebic biology. Based on other works, ATPase
388 activity of C-terminal EHD-containing proteins is crucial for various stages of the endocytic
389 traffic machinery. Hydrolysis of ATP was essential for binding of human EHD2 complexes

to caveolae during clathrin-independent endocytosis (39). It is suggested that membrane scission results from ATP hydrolysis by human EHD2 in vivo (35). Using cross-complementation assays in *C. elegans*, ATP binding and hydrolysis of human EHD1 was essential for endocytic recycling. It was also shown using in vitro liposome-based assays that ATP binding of human EHD1 promote scaffold self-assembly, while ATP hydrolysis enables extension of bulges and thinning of tubular model membranes which leads to scission (40). In vitro analysis also revealed that ATP binding and concomitant hydrolysis allows membrane remodelling into highly curved tubules (29). We can only hypothesize that ATP hydrolysis in amoebic EHD1 may have functions similar to its homologs in other organisms.

We also detected *Eh*EHD1 in the phagocytic cup, and membranes of phagosomes and trogosomes, although only a select few phagosomes and trogosomes are labeled with EhEHD1 in both live and fixed imaging analysis. The same can also be said when we performed endocytosis assay using either RITC-dextran or Alexa Fluor 568-transferrin. This suggests the nature of EHD localization being dependent on either recruitment by interacting proteins or association/binding with certain lipids on vesicular membranes at specific time points. This is reflected by the localization of either GFP-EHD1 or HA-EHD1 in membranes of vesicles of various sizes, and the seemingly polarized signal intensity onto sites where two vesicles are in close contact.

As suggested by our lipid overlay assay result, *Eh*EHD1 preferentially binds to PI(3,5)P2 and PI(4,5)P2. PI(4,5)P_2 has been demonstrated to be localized to the plasma membrane (41), lipid rafts and uroids (42) of *E. histolytica.* It is important to note that PI(4,5)P2 localized at the plasma membrane is involved initiating internalization during

endocytosis, micropinocytosis, and phagocytosis (43, 44), whereas PI(3,5)P2 has a critical role in endosome/lysosome biogenesis, and in the initiation of MVB formation (45). Together, these results circumstantially support our observations of amoebic EHD1 localization and involvement in early endosome, intraluminal vesicle, and MVB formation.

On the possible role(s) of mitosome-endosome contact in *E. histolytica*, we posit that this MCS may be involved in lipid transfer, ion transport, and quality control. Lipid transport and/or metabolism are commonly alluded roles of MCSs. Although we did not detect any lipid transport proteins in our immunoprecipitation assay, two lipid transport proteins (LTP1 and LTP3) in *E. histolytica* have been characterized (46), and it is plausible that various LTPs may transiently interact with amoebic MCSs to facilitate lipid mobility across organelles. We detected a few fatty acid ligases in the ~90 and ~180 kDa complex, however the interaction of these proteins to the HA-ETMP1 containing complex needs to be experimentally validated. Alternatively, ion transport may also be facilitated in this MCS, as was demonstrated in epithelial cells, where the mitochondria and endosomes that contain iron-bound transferrin are involved in “kiss and run” interactions, leading to iron transfer from endosomes to mitochondria (47). Another possibility is the involvement of EHD1 in mitosomal dynamics. Mitochondria undergo dynamics of fusion and fission to ensure maintenance of homeostasis, control of reactive oxygen species, apoptosis, and autophagy. Dynamin and dynamin related proteins (Drps) have been implicated in mitochondrial fission. Recently in HeLa cells, EHD1 was reported to be a novel regulator of mitochondrial fission via a mechanism distinct from that of dynamin/Drp. In this model human EHD1, together with its binding partner rabankyrin-5 interact with the retromer complex participate in mitochondrial division. EHD1 was suggested to facilitate the fission

436 of vesicles that transport Vps35, a retromer complex component, from endosomes to the
437 mitochondrial membrane. It was also suggested that Vps35 may interact with inactive
438 Drp1 on the mitochondrial membrane, causing its removal and subsequent action of
439 active Drp1 to perform mitochondrial fission (48). Fission has also been reported in MROs
440 of anaerobic parasites such as the hydrogenosomes of *Trichomonas vaginalis* and *E.*
441 *histolytica* (49–51). Mitosome fission in *E. histolytica* was reported to involve a
442 heterodimer complex of two dynamin-related proteins, DrpA and DrpB (50). It is
443 interesting if amoebic EHD1 also takes part in influencing mitosome fission as was
444 postulated in mammalian cells (48). An alternative novel pathway for mitochondrial quality
445 control that is independent of Atg5 and LC3 is the formation of mitochondria-derived
446 vesicles targeted to lysosomes. Ultrastructural analysis of COS7 cells identified the
447 presence vesicles that are Tom20-positive within MVBs (52). Furthermore, in hepatocytes,
448 a complex made up of EHD2, EH domain binding protein 1 (EHBP1), and Rab10,
449 promotes extension of the LC3-containing autophagic membrane in order to engulf lipid
450 droplets during lipophagy (53). Such related pathways may also exist in *E. histolytica* that
451 warrants further investigation in the future.
452
453 **Conclusion**
454 We report a novel membrane contact site between mitosomes and endosomes of
455 *Entamoeba histolytica*. This unprecedented MCS features the mitosomal membrane
456 protein ETMP1 and a C-terminal EH domain containing protein, EHD1. ETMP1 is a
457 protein unique to *Entamoeba* and is essential to parasite proliferation. It interacts with
458 EHD1, a protein involved in various endocytic processes in *E. histolytica*, namely in early

459 endosome formation during bulk and receptor-mediated endocytosis, phagocytosis and
460 trogocytosis of mammalian cells, and in the invagination of intraluminal vesicles for the
461 generation of multivesicular bodies. Such novel ETMP1-EHD1 interaction hints at a
462 possible role of this mitosome-endosome MCS on various physiological processes that
463 have been demonstrated in other organisms. We thus propose that ETMP1-EHD1
464 mediated contact site is involved in lipid transfer, biogenesis, autophagy, organelle
465 dynamics and quality control of MROs. Further investigation is needed to fully dissect the
466 molecular mechanisms and functions of this and other MRO-related MCSs.
467

468 **Materials and Methods**

469 ***Entamoeba histolytica* cultivation**

470 *Entamoeba histolytica* HM-1:IMSS Cl6 (54) and G3 (55) strains were maintained
471 in Diamond's BI-S-33 medium (54) as described previously. Subculture was performed
472 after incubation of up to 3-4 days when trophozoites reached the late-logarithmic phase.

473 **Plasmid construction**

474 Extraction of total RNA from *E. histolytica* trophozoites, purification of mRNA, and
475 synthesis of cDNA were performed by following protocols described previously (24). For
476 the expression of hemagglutinin (HA) tagged proteins in *E. histolytica* trophozoites, target
477 genes (*etmp1*: EHI_175060 and *ehd1*: EHI_105270) were amplified by polymerase chain
478 reaction (PCR) using *E. histolytica* cDNA as template, and the corresponding primer sets:
479 (etmp1-*Xma*I-fwd: GTTcccgggATGGAACAAATAACTGAAGAA; *etmp1-Xho*I-rev:
480 GAActcgagTTATTTTTTCATTTTTCTTAAGG; and *ehd1-Xma*I-fwd:
481 GTTcccgggATGTTTGGTAAGAAGAAACAAAAACC; *ehd1-Xho*I-rev:

GAActcgagTTATTCAACTGGTGGAAGATTGTC). These PCR amplicons were inserted into the following plasmids: pEhEx-HA and pEhEx-GFP for constitutive expression, (56) and pEhtEx-HA and pEhtEx-GFP for tetracycline-induced expression (50), after digestion with *Xma*I and *Xho*I (New England Biolabs, Beverly, MA, USA) and then ligated using Ligation Convenience Kit (Nippongene, Tokyo, Japan). For the expression of recombinant proteins in *Escherichia coli*, PCR-amplification of *ehd1* was performed using *E. histolytica* cDNA as template and the following primer set (*ehd1*-*Bam*HI-fwd: GTTggatccATGTTTGGTAAGAAGAAACAAAAACC, and *ehd1*-*Sal*I-rev: GAAgtcgacTTATTCAACTGGTGGAAGATTGTC). Digestion and ligation to *Bam*HI and *Sal*I-linearized pColdI plasmid (Takara, Shiga, Japan) were performed. For transcriptional gene silencing, about 400 bp fragments of *etmp1* and *ehd1* were amplified using cDNA and appropriate primer sets: etmp1gs-*Stu*I-fwd: GTTaggcttATGGAACAAATAACTGAAG; etmp1gs-*Sac*I-rev: GAAgagctcCTAATTTGATTCCTTTTAAAG; and ehd1gs-*Stu*I-fwd: GTTaggcctATGTTTGGTAAGAAGAAACAA and ehd1gs-*Sac*I-rev: GAAgagctcTAAATTTAGCCATAAATTCAT. The amplicons were digested with *Stu*I and *Sac*I and ligated to pSAP2-Gunma (57).

Amoeba transfection and drug selection

The constructed plasmids described above were transfected by lipofection into *E. histolytica* trophozoites, as described previously (58, 59). Selection of transfectants was performed by changing the culture medium supplemented with G418 (Gibco/Life Technologies, USA) for those transfected with pEhEx-based plasmids, or with hygromycin (Fujifilm Wako, Japan) for those transfected with pEhtEx-based plasmids. The starting concentration of either 1 μg/mL G418 or hygromycin added was gradually

505 increased until all control cells (transfected without plasmid) died from the antibiotic
506 challenge. All resultant strains were maintained in medium containing 10 µg/mL G418 or
507 20 µg/mL hygromycin unless otherwise stated. For tetracycline-induction of protein
508 expression, 10 µg/mL tetracycline was added to semi-confluent cultures 24 h prior to
509 performing assays unless otherwise stated.

510 **Immunoflourescence assay (IFA)**

511 Double-staining immunofluorescence assay was performed as previously
512 described (13), using anti-HA mouse monoclonal antibody (clone 11MO, Covance, USA)
513 diluted 1:500 in 2% saponin and 0.1% bovine serum albumin in phosphate buffered saline
514 (saponin-BSA-PBS), to detect HA-tagged ETMP1 and EHD1, respectively, and one of the
515 following polyclonal rabbit antisera diluted 1:1000 in saponin-BSA-PBS unless otherwise
516 stated: anti-adenosine-5'-phosphosulfate kinase (APSK; EHI_179080; a mitosomal
517 matrix protein; (57) diluted 1:300; anti- vacuolar protein sorting 26 (Vps26; EHI_062490;
518 a retromer complex component (19)); anti-Rab11B (EHI_107250; involved in cysteine
519 protease secretion; (22)); and anti-pyridine nucleotide transhydrogenase (PNT;
520 EHI_014030; a novel class of lysosomal PNT; (21)). Secondary antibodies used were
521 Alexa Fluor-488 anti-mouse antibody and Alexa Fluor-568 anti-rabbit antibody Thermo
522 Fisher diluted 1:1000 in saponin-BSA-PBS, respectively. Cells were visualized using
523 LSM780 (Carl Zeiss Microscopy, Germany) confocal laser scanning microscope.

524 **Subcellular fractionation and immunoblot analysis**

525 Trophozoites at the late-logarithmic phase were collected and washed thrice with
526 2% glucose-PBS. Cells were mechanically disrupted using a Dounce homogenizer as
527 described previously (13). The resulting homogenate was separated by Percoll-gradient

fractionation as previously described (13, 18). For carbonate fractionation, organelle-enriched fractions from HA-ETMP1, MBOMP30-HA, HA-EHD1 and mock control homogenates were collected by centrifugation at 100,000 *g* for 60 min at 4°C. The resultant pellet was reacted with sodium carbonate as previously described (13, 23, 24). All fractions collected were run in SDS-PAGE followed by Western blotting as previously described (60). Immunostaining of PVDF membranes was performed using anti-HA antibody, anti-APSK antiserum (organelle fraction marker), anti-cysteine synthase 1 (CS1; EHI_171750; cytosolic enzyme involved in cysteine metabolism) (61), anti-cysteine protease binding family protein 1 (CPBF1; EHI_164800, membrane fraction control) (62) and chemiluminescent bands were visualized using LAS-4000 mini luminescent image analyzer (Fujifilm Life Science, Tokyo, Japan).

In silico predictions and analyses

Transmembrane domain-containing mitosomal proteins were predicted using a pipeline developed in our previous study (12). To search for homologs of ETMP1 in various *Entamoeba* species, we used as query the *E. histolytica* protein, EHI_175060, and implemented a BLAST search using the *Amoebozoa* resource database, AmoebaDB (63). Coiled-coil regions were predicted using DeepCoil (64).

Immunoelectron microscopy

Samples were prepared as described previously (24). The specimens were double-stained with anti-HA mouse antibody, and anti-APSK rabbit antiserum (57). Processing and visualization were performed by Tokai Microscopy Inc. (Nagoya, Japan), using a transmission electron microscope (JEM-1400 Plus, JEOL Ltd., Japan) at an

acceleration voltage of 80 kV. Digital images with a resolution of 2048 × 2048 pixels were taken using a CCD camera (VELETA, Olympus Soft Imaging Solution GmbH, Germany).

Immunoprecipitation (IP) of HA-ETMP1 by anti-HA antibody

Organelle-enriched fractions from HA-ETMP1 and mock pEhEx-HA control homogenates were prepared and approximately 2 µg of proteins were solubilized in 2% digitonin in IP Buffer containing 50 mM BisTris-HCl, pH 7.2, 50 mM NaCl, 0.001 % Ponceau S, and 10 % w/v glycerol for 30 min on ice. The solubilized fraction was collected by centrifugation at 20,000 *g* for 30 min at 4 °C. Immunoprecipitation was performed as previously described (23). Bound proteins were eluted overnight using 60 µg HA peptide. Eluted fractions were loaded on SDS-PAGE gels, followed by immunoblotting using mouse anti-HA antibody. Silver staining was performed using the Silver Stain MS kit (Fujifilm Wako Pure Chemical Corporation, Osaka, Japan), according to the manufacturer's protocol. Protein sequencing by liquid chromatography-mass spectrometry analysis was conducted by the Biomolecular Analysis Facility Core, University of Virginia.

Lipid overlay assay

As described previously (20), the lysate of HA-EHD1 expressing strain was used to probe a P-6001 phospholipid membrane strip (Echelon Biosciences, Salt Lake City, Utah, USA). The lysate of HA-SNX1 which binds to PI3P (20) was used as a positive control. The strips were washed three times with 0.1% Tween 20 in PBS (PBS-T), followed by reaction with 1:1000 anti-HA mouse antibody in 3% BSA-PBS for 2 h at room temperature. The strips were washed and incubated with 1:6000 HRP-conjugated goat anti-mouse IgG (Thermo-Fisher Scientific, USA) in 3% BSA-PBS for 1 h at room

573 temperature. Finally, the strips were washed and reacted with the Immobilon ECL Ultra
574 Western HRP Substrate (Millipore, USA) following manufacturer's instructions.

575 **Endocytosis assay**

576 Approximately 1×10^5 GFP-EHD1 or mock-GFP expressing trophozoites in 1 mL
577 BI-S-33 of strains respectively were placed on a 35 mm collagen-coated glass- bottom
578 culture dish (MatTek Corporation, Ashland, MA) for 15 minutes to allow for cell attachment.
579 The medium was removed and replaced with 1 mL of BI-S-33 supplemented with either
580 2 mg/mL RITC-dextran (MW = 70 000; Sigma-Aldrich, USA) or 100 µg/ml Alexa Fluor-
581 568 transferrin (Thermo-Fisher Scientific, USA). Chase was performed for up to 30 min
582 for live imaging. For IFA, fixation was conducted onto HA-EHD1 and mock-HA strains
583 after 0, 30, 60, 120 min of addition of either RITC-dextran or Alexa Fluor 568-transferrin.
584 Images were captured using a confocal laser scanning microscope LSM780 (Carl Zeiss
585 Microscopy, Germany), as the cells were being incubated at 35 °C using a temperature-
586 controlled stage plate (Carl Zeiss Microscopy, Germany).

587 **Phagocytosis assay**

588 A semi-confluent culture of Chinese hamster ovary (CHO) cells, grown in F12
589 medium (Sigma-Aldrich, USA) was stained by addition of 40 µM CellTracker Blue
590 (Thermo-Fisher Scientific, USA) for 30 min at 37°C. The medium containing excess dye
591 was removed and the cells were washed in 1X PBS followed by treatment with 0.1%
592 trypsin for 5 min at 37°C. The detached cells were collected and washed with 1X PBS
593 thrice by centrifugation at 3000 rpm for 3 minutes. Stained CHO cells were resuspended
594 in BI-S-33 medium prior to addition to amoeba cells. Cells were co-incubated for 15, 30,
595 and 60 min respectively, after which they were fixed for IFA analysis as mentioned above,

596 but using anti-GFP antibody (Sigma-Aldrich, USA) and anti-Vps26 antiserum respectively.
597 A parallel setup was prepared for live imaging analysis.

598 **Expression and purification of recombinant His-EHD1**

599 *Escherichia coli* BL21 strain was transformed using the pCold-His-EHD1 plasmid
600 described above, and the transformants were selected using LB agar containing 150
601 µg/ml of ampicillin. Isolated colonies were cultured in LB medium with 150 µg/ml of
602 ampicillin, incubated at 37 °C with shaking. A 1L culture was inoculated and incubated in
603 a shaker at 37 °C until reaching optical density (OD) 600 of 0.7. The culture was flash
604 cooled in an ice water bath for 30 minutes. Induction of protein expression was made by
605 adding 0.5 mM isopropyl β-D-thiogalactopyranoside (IPTG) to the medium followed by
606 incubation at 15 °C with shaking for 24 h. Cells were collected and protein expression
607 was confirmed by loading the soluble and insoluble fractions in SDS-PAGE followed by
608 Coomassie blue staining and anti-His immunoblot analysis respectively as described
609 previously (65). His-EHD1 was purified by binding with Ni^{2+}-NTA His-bind slurry (Qiagen,
610 Germany) and eluting with imidazole as described previously (65). Purified His-EHD1 was
611 stored at -80°C with 20% glycerol in small aliquots until use.

612 **Enzyme activity assay**

613 Varying amounts of purified His-EHD1 (0, 0.125, 0.25, 0.5, 1.0 µg) were
614 resuspended in assay buffer (20 mM HEPES pH 7.5, 0.005 % Tween 20, 10 % glycerol,
615 1 mM DTT, 20 mM NaCl, and 10 mM $MgCl_2$) and loaded triplicate onto independent wells
616 of a 96-well plate. Then, 2 µl of 100 mM ATP was used as substrate and distilled water
617 was added to bring the volume of the mixture to 20 µl. Finally, 20 µl of 2X stock solution
618 (66) containing 100 mM Tris-HCl (pH 7.5), 10 mM $MgCl_2$, 0.02% Triton X-100, 0.01%

BSA, 2 mM glucose, 0.2 mM NADP, 2 u/mL ADP-hexokinase, 2 U/mL glucose-6-phosphate dehydrogenase, 2 U/mL diaphorase I, 0.1 mM resazurin in DMSO, and 20 mM N-ethylmaleimide in DMSO, was added and the plate was incubated at 37 °C for 30 min. For determining kinetic parameters, 0, 12.5, 25, 50, 75, 100, 125, 250, 500, 750, 1000, and 2500 μM ATP was used to react with 1.5 μg His-EHD1 for 30 min. The fluorescence was measured continuously at excitation and emission wavelengths of 540 nm and 590nm, respectively using SpectraMax Paradigm Multi-Mode microplate reader (Molecular Devices, San Jose, CA, USA).

Manuscript word count: 6,531 words

Acknowledgments

This research is funded by Grants-in-Aid for Scientific Research (B) (JP18H02650 and JP21H02723 to T.N.), Grants-in-Aid for Young Scientists (JP20K16233 to H.J.S.) and Core-to-Core Program, (JPJSCCB20190010) from the Japan Society for the Promotion of Science, Grant for research on emerging and re-emerging infectious diseases from Japan Agency for Medical Research and Development (AMED, JP20fk0108138 to T.N.). The authors want to thank Mihoko Imada of The University of Tokyo for her techincal support. The authors also want to thank Dr. Takashi Makiuchi of Tokai University School of Medicine, Japan, and Dr. Eri Hayakawa of Jichi Medical University, Japan for their valuable discussion.

Conflict of interest: The authors declare no conflict of interest.

Figure Legends

Figure 1

Multiple sequence alignment of ETMP1 orthologs in *Entamoeba*. Amino acid sequences of orthologs in *E. histolytica* (EHI_175060), *E. nutttalli* (ENU1_040700), *E. dispar* (EDI_139180), and *E. moshkovskii* (EMO_001640) were aligned using MAFFT (67), and displayed using Jalview (68). The hydrophobic, positively charged, negatively charged, polar, cysteine, glycine, proline, aromatic residues are indicated in blue, red, magenta, green, pink, orange, yellow, and cyan respectively. Dashed black boxes show predicted coiled coil domains by DeepCoil (64), while the dashed red box indicates the predicted transmembrane region by our TMD prediction tool (12).

Figure 2

Expression and localization of HA-ETMP1 in *E. histolytica* trophozoites. (A) Approximately 30 µg protein from whole cell lysates of HA-ETMP1 and mock control (pEhEx-HA) strains were separated by SDS-PAGE and subjected to anti-HA immunoblot analysis. The 33 kDa band corresponds to the predicted molecular mass of HA-ETMP1 (white arrowhead). (b) Immunofluorescence analysis of HA-ETMP1-expressing trophozoites, double stained with anti-HA (green) and anti-APSK (red) respectively. Scale bar = 10 µm. (C) Fractionation of HA-ETMP1 by discontinuous Percoll-gradient ultracentrifugation. Homogenate of HA-ETMP1 was separated by density against a Percoll gradient. Approximately 15 µL of fractions collected from the first (1 to 22) and second (A to V) ultracentrifugation steps were separated by SDS-PAGE followed by immunoblot analysis with anti-HA and anti-Cpn60 antibodies respectively. (D) Anti-HA and anti-Cpn60 immunoblot profiles of subcellular fractionation including alkaline carbonate treated organelle-rich fractions of HA-ETMP1 and HA-MBOMP30 (mitosome

membrane control) respectively. (E) Representative immunoelectron micrographs of 15 nm anti-APSK gold-labeled mitosomes of HA-ETMP1, co-stained with 5 nm anti-HA gold. Scale bar = 200 nm.

Figure 3

Growth curve of HA-ETMP1 and mock-HA strain. Cell numbers of ETMP1 (black line) and mock-HA strain (red line) cultivated in BI-S-33 medium containing 0, 10, and 20 µg/mL G418 respectively, were plotted against time (h). Western blot analysis of whole cell lysates of HA-ETMP1 and mock-HA grown in medium containing 0, 10, and 20 µg/mL G418, and harvested at various time points. Upper and lower panels show anti-HA and anti-CPBF1 (loading control) immunoblots respectively.

Figure 4

Anti-HA beads immunoprecipitation (IP) of mock-HA and HA-ETMP1 strains. (A) Western blot analysis using anti-HA antibody of the cell lysates and various IP fractions of HA- mock-HA (left) and ETMP1 (right) respectively. A black arrowhead indicates the position of HA-tagged ETMP1 (33 kDa). (B) Silver stained-SDS-PAGE gel of IP eluates of mock-HA and HA-ETMP1 strains respectively. A black arrowhead points to a specific ~55 kDa band unique to HA-ETMP1. (C) Enriched or exclusively detected proteins in the ~55 kDa excised gel band from HA-ETMP1 IP eluate as compared to that of mock-HA control IP eluate by LC-MS/MS sequencing analysis. MW stands for predicted molecular weight. QV denotes quantitative values (normalized total spectra). Presence of the detected proteins in the previously published mitosome proteome data (Mi-ichi et al., 2009) was performed and the result listed in the last column (+ indicates presence, - indicates absence). (D) Total cell lysates of mock-HA and ETMP1 respectively were

688 separated by BN-PAGE, followed by anti-HA Western blot analysis. Black and red
689 arrowheads respectively indicate the ~180 kDa and ~90 kDa complexes that contain HA-
690 ETMP1.

691 **Figure 5**

692 **HA-EHD1 expression in *E. histolytica* trophozoites.** (A) Anti-HA immunoblot analysis
693 of approximately 30 µg total cell lysates of mock-HA and HA-EHD1, respectively, show a
694 61 kDa band corresponding to HA-tagged EHD1. (B-C) Representative
695 immunofluorescence images of fixed HA-EHD1 expressing cells double-stained with anti-
696 HA (green) and anti-APSK (red) antibodies respectively. White arrow and arrowheads
697 indicate proximity and colocalization between anti-HA and anti-APSK signals respectively.
698 Scale bar = 10 µm. (D) Representative immunoelectron micrographs of HA-EHD1
699 trophozoites, double stained with 5 nm anti-HA gold and 15 nm anti-APSK gold. Scale
700 bar = 200 nm. The letters “c”, “e”, and “m” indicate cytosol, endosomes, and mitosomes,
701 respectively. An arrowhead points to the structure where the membranes of the mitosome
702 and endosome are in close contact. (E) Percoll-gradient fractionation of HA-EHD1
703 followed by western blot analysis using anti-HA and ant-Cpn60 antibodies respectively.

704 **Figure 6**

705 **Association of HA-EHD1 to *E. histolytica* membranes.** (A) Colocalization analysis of
706 HA-EHD1 with various endosomal markers. Representative IFA images HA-EHD1 co-
707 stained with anti-HA (green) and anti-vacuolar protein sorting 26 (Vps26, red, upper
708 panel), anti-pyridine nucleotide transhydrogenase (PNT, red, middle panel), and anti-
709 Rab11B (red, bottom panel) respectively. (B) Immunoblot analysis of carbonate
710 fractionation assay of HA-EHD1 organelle-rich fraction using (from top to bottom panel)

anti-HA, anti-CS1 (cytosolic protein control) anti-Sec13 (peripheral membrane protein control), and anti-CPBF1 (membrane protein control) respectively. (C) Lipid overlay assay of HA-EHD1 and HA-SNX1 (PI3P binding protein control) respectively. The membrane strips contain 100 pmol of the following lipids per spot: lysophosphatidic acid (LPA), lysophosphocholine (LPC), phosphatidylinositol (PtdIns), phosphatidylinositol (3)-phosphate (PtdIns(3)P), phosphatidylinositol (4)-phosphate (PtdIns(4)P), phosphatidylinositol (5)-phosphate (PtdIns(5)P), phosphatidylethanolamine (PE) phosphatidylcholine (PC), sphingosine 1-phosphate (S1P), phosphatidylinositol (3,4)-bisphosphate (PtdIns(3,4)P2), phosphatidylinositol (3,5)-bisphosphate (PtdIns(3,5)P2), phosphatidylinositol (4,5)-bisphosphate (PtdIns(4,5)P2), phosphatidylinositol (3,4,5)-trisphosphate (PtdIns(3,4,5)P3), phosphatidic acid (PA), phosphatidylserine (PS) respectively.

Figure 7

Involvement of HA-EHD1 in multivesicular body formation. (A) Representative anti-HA antibody and anti-APSK antiserum (upper panel) or anti-Vps26 antiserum (lower panel) double-staining IFA images of trophozoites that expressed HA-EHD1 trophozoites after 1h, 3h, and 24h of induction by tetracycline. Scale bar = 10 μm. (B) Representative immunoelectron image of trophozoite expressing HA-EHD1 24 h post-tetracycline induction, stained with 15 nm gold anti-HA. The initials “c”, “MVB”, and “ILV” denote cytosol, multivesicular body and intraluminal vesicle, respectively. Scale bar = 200 nm.

Figure 8

Involvement of GFP-EHD1 in amoebic endocytosis. (A) Anti-GFP immunoblot analysis of approximately 20 μg total lysate of GFP-EHD1 expressing trophozoite. (B) Confocal

734 microscopy images from movies of live trophozoites expressing GFP-EHD1 (left panel),
735 and GFP-EHD1 in medium supplemented with either RITC-dextran (middle panel) or
736 Alexa Fluor 568-transferrin (right panel) respectively. Scale bar = 10 μm.

737 **Figure 9**

738 **Involvement of HA-EHD1 in amoebic phagocytosis and trogocytosis.**
739 Representative IFA images of fixed anti-HA (green) and anti-Vps26 (red) double-stained
740 HA-EHD1 trophozoites 15, 30, and 60 minutes (top to bottom) after coincubation with
741 CellTracker Blue-stained Chinese hamster ovary (CHO) cells.

742 **Figure 10**

743 **Activity assay of purified recombinant His-EHD1.** (A) Coomassie Brilliant Blue-stained
744 SDS-PAGE gel (left panel) and anti-His immunoblot (right panel) of purification fractions
745 of His-EHD1. (C) Determination of the specific activity of His-EHD1 using ATP as
746 substrate at various concentrations.

747

748 **Supplemental Materials**

749 **Supplementary Movie S1**

750 Multiple z-section images of fixed HA-EHD1, 24 h after tetracycline induction. Green and
751 red signals indicate anti-HA and anti-APSK antibodies respectively. Scale bar = 5 μm.

752 **Supplementary Movie S2**

753 Live imaging of GFP-EHD1 after 24 of tetracycline induction. Scale bar = 5 μm.

754 **Supplementary Movie S3**

Live imaging of GFP-EHD1 trophozoites chased a few minutes after addition of RITC-dextran. Note the recruitment of GFP-EHD1 in newly closed endosomes. Scale bar = 5 μm.

Supplementary Movie S4

Live imaging of GFP-EHD1 trophozoites chased a few minutes after addition of Alexa Fluor 568-transferrin. Note the recruitment of GFP-EHD1 in newly closed endosomes.

Supplementary Movie S5

Live imaging of GFP-EHD1 trophozoites chased a few minutes after addition of Alexa Fluor 568-transferrin. Note the accumulation of GFP-EHD1 in the plasma membrane where aggregated transferrin is located. Scale bar = 5 μm.

Supplementary Movie S6

Multiple z-section images of fixed GFP-EHD1, (60 min after co-incubation with CellTracker blue-stained Chinese hamster ovary cells. Scale bar = 5 μm.

Supplementary Movie S7

Live imaging of GFP-EHD1 trophozoites chased a few minutes after co-incubation with CellTracker blue-stained Chinese hamster ovary cells. Scale bar = 5 μm.

Supplementary Figure S1

Anti-HA immunoprecipitation of HA-EHD1 and mock-HA control. (A) Western blot analysis of various IP fractions probed using anti-HA antibody (B) Silver-stained SDS-PAGE gel showing separated protein bands from eluted IP samples. Black boxes indicated regions excised and submitted for subsequent protein sequencing analysis.

Supplementary Table S1

(A) Exclusively detected proteins in the ~180 kDa excised blue-native PAGE gel band from HA-ETMP1 as compared to that of mock-HA control by LC-MS/MS sequencing analysis. MW indicates predicted molecular weight, while QV denotes quantitative values (normalized total spectra). (B) Detected proteins in the ~180 kDa excised blue-native PAGE gel band enriched in HA-ETMP1 as compared to that of mock-HA control by LC-MS/MS sequencing analysis (Qv HA/ETMp1/mock-HA ≥ 2.0.) (C) Exclusively detected proteins in the ~90 kDa excised blue-native PAGE gel band enriched in HA-ETMP1 as compared to that of mock-HA control by LC-MS/MS sequencing analysis.

Supplementary Table S2

(A) Proteins identified in the 55-58 kDa excised gel band of HA-EHD1 and mock-HA IP eluate samples respectively, by LC-MS/MS analysis. MW indicates predicted molecular weight, while QV denotes quantitative values (normalized total spectra). (B) Proteins identified in the 30-33 kDa excised gel band of HA-EHD1 and mock-HA IP respectively, by LC-MS/MS analysis. MW indicates predicted molecular weight, while QV denotes quantitative values (normalized total spectra).

References

1. Jain A, Holthuis JCM. 2017. Membrane contact sites, ancient and central hubs of cellular lipid logistics. Biochim Biophys Acta - Mol Cell Res 1864:1450–1458.
2. Helle SCJ, Kanfer G, Kolar K, Lang A, Michel AH, Kornmann B. 2013. Organization and function of membrane contact sites. Biochim Biophys Acta - Mol Cell Res 1833:2526–2541.

3. Scorrano L, De Matteis MA, Emr S, Giordano F, Hajnóczky G, Kornmann B, Lackner LL, Levine TP, Pellegrini L, Reinisch K, Rizzuto R, Simmen T, Stenmark H, Ungermann C, Schuldiner M. 2019. Coming together to define membrane contact sites. Nat Commun 10:1–11.

4. Hoyer MJ, Chitwood PJ, Ebmeier CC, Striepen JF, Qi RZ, Old WM, Voeltz GK. 2018. A novel class of ER membrane proteins regulates ER-associated endosome fission. Cell 175:254–265.

5. Wong YC, Ysselstein D, Krainc D. 2018. Mitochondria-lysosome contacts regulate mitochondrial fission via RAB7 GTP hydrolysis. Nature 554:382–386.

6. Stanley SL. 2003. Amoebiasis. Lancet 361:1025–1034.

7. Santos HJ, Makiuchi T, Nozaki T. 2018. Reinventing an Organelle: The Reduced Mitochondrion in Parasitic Protists. Trends Parasitol 1–18.

8. Mi-ichi F, Miyamoto T, Takao S, Jeelani G, Hashimoto T, Hara H, Nozaki T, Yoshida H. 2015. *Entamoeba* mitosomes play an important role in encystation by association with cholesteryl sulfate synthesis. Proc Natl Acad Sci 112:E2884–E2890.

9. Teixeira JE, Huston CD. 2008. Evidence of a continuous endoplasmic reticulum in the protozoan parasite Entamoeba histolytica 7:1222–1226.

10. Perdomo D, Aït-Ammar N, Syan S, Sachse M, Jhingan GD, Guillén N. 2015. Cellular and proteomics analysis of the endomembrane system from the unicellular Entamoeba histolytica. J Proteomics 112:125–140.

11. Santos HJ, Imai K, Makiuchi T, Tomii K, Horton P, Nozawa A, Okada K, Tozawa Y, Nozaki T. 2019. Novel lineage-specific transmembrane β-barrel proteins in the

endoplasmic reticulum of Entamoeba histolytica. FEBS J 286:3416–3432.

12. Santos HJ, Imai K, Hanadate Y, Fukasawa Y, Oda T, Mi-ichi F, Nozaki T. 2016. Screening and discovery of lineage-specific mitosomal membrane proteins in Entamoeba histolytica. Mol Biochem Parasitol 209:10–17.

13. Santos HJ, Hanadate Y, Imai K, Nozaki T. 2019. An Entamoeba-Specific Mitosomal Membrane Protein with Potential Association to the Golgi Apparatus. Genes (Basel) 10:367.

14. Santos HJ, Nozaki T. 2021. Interorganellar communication and membrane contact sites in protozoan parasites. Parasitol Int 83:102372.

15. Saito-Nakano Y, Loftus BJ, Hall N, Nozaki T. 2005. The diversity of Rab GTPases in Entamoeba histolytica. Exp Parasitol 110:244–252.

16. Lopez-Reyes I, García-Rivera G, Bauelos C, Herranz S, Vincent O, Lpez-Camarillo C, Marchat LA, Orozco E. 2010. Detection of the endosomal sorting complex required for transport in entamoeba histolytica and characterization of the EhVps4 protein. J Biomed Biotechnol 2010.

17. Avalos-Padilla Y, Knorr RL, Javier-Reyna R, García-Rivera G, Lipowsky R, Dimova R, Orozco E. 2018. The Conserved ESCRT-III Machinery Participates in the Phagocytosis of Entamoeba histolytica. Front Cell Infect Microbiol 8:1–17.

18. Mi-ichi F, Yousuf MA, Nakada-Tsukui K, Nozaki T. 2009. Mitosomes in Entamoeba histolytica contain a sulfate activation pathway. Proc Natl Acad Sci 106:21731–21736.

19. Nakada-Tsukui K, Saito-Nakano Y, Ali V, Nozaki T. 2005. A retromerlike complex is a novel Rab7 effector that is involved in the transport of the virulence factor

cysteine protease in the enteric protozoan parasite Entamoeba histolytica. Mol Biol Cell2005/08/27. 16:5294–5303.

20. Watanabe N, Nakada-Tsukui K, Nozaki T. 2020. Two isotypes of phosphatidylinositol 3-phosphate-binding sorting nexins play distinct roles in trogocytosis in Entamoeba histolytica. Cell Microbiol 22:1–16.

21. Yousuf MA, Mi-Ichi F, Nakada-Tsukui K, Nozaki T. 2010. Localization and targeting of an unusual pyridine nucleotide transhydrogenase in Entamoeba histolytica. Eukaryot Cell 9:926–933.

22. Mitra BN, Saito-Nakano Y, Nakada-Tsukui K, Sato D, Nozaki T. 2007. Rab11B small GTPase regulates secretion of cysteine proteases in the enteric protozoan parasite Entamoeba histolytica. Cell Microbiol 9:2112–2125.

23. Makiuchi T, Mi-ichi F, Nakada-Tsukui K, Nozaki T. 2013. Novel TPR-containing subunit of TOM complex functions as cytosolic receptor for Entamoeba mitosomal transport. Sci Rep 3:1129.

24. Santos HJ, Imai K, Makiuchi T, Tomii K, Horton P, Nozawa A, Ibrahim M, Tozawa Y, Nozaki T. 2015. A novel mitosomal β-barrel outer membrane protein in Entamoeba. Sci Rep 5:1–10.

25. Galperin E, Benjamin S, Rapaport DD, Rotem-Yehudar R, Tolchinsky S, Horowitz M. 2002. EHD3: A protein that resides in recycling tubular and vesicular membrane structures and interacts with EHD1. Traffic 3:575–589.

26. George M, Ying GG, Rainey MA, Solomon A, Parikh PT, Gao Q, Band V, Band H. 2007. Shared as well as distinct roles of EHD proteins revealed by biochemical and functional comparisons in mammalian cells and C. elegans. BMC Cell Biol

8:1–22.

27. Confalonieri S, Di Fiore PP. 2002. The Eps15 homology (EH) domain. FEBS Lett 513:24–29.

28. Yeow I, Howard G, Chadwick J, Mendoza-Topaz C, Hansen CG, Nichols BJ, Shvets E. 2017. EHD Proteins Cooperate to Generate Caveolar Clusters and to Maintain Caveolae during Repeated Mechanical Stress. Curr Biol 27:2951-2962.e5.

29. Melo AA, Hegde BG, Shah C, Larsson E, Isas JM, Kunz S, Lundmark R, Langen R, Daumke O. 2017. Structural insights into the activation mechanism of dynamin-like EHD ATPases. Proc Natl Acad Sci U S A 114:5629–5634.

30. Naslavsky N, Rahajeng J, Rapaport D, Horowitz M, Caplan S. 2007. EHD1 regulates cholesterol homeostasis and lipid droplet storage. Biochem Biophys Res Commun 357:792–799.

31. Bar M, Aharon M, Benjamin S, Rotblat B, Horowitz M, Avni A. 2008. AtEHDs, novel Arabidopsis EH-domain-containing proteins involved in endocytosis. Plant J 55:1025–1038.

32. Lin SX, Grant B, Hirsh D, Maxfield FR. 2001. Rme-1 regulates the distribution and function of the endocytic recycling compartment in mammalian cells. Nat Cell Biol 3:567–572.

33. Thakur V, Asad M, Jain S, Hossain ME, Gupta A, Kaur I, Rathore S, Ali S, Khan NJ, Mohmmed A. 2015. Eps15 homology domain containing protein of Plasmodium falciparum (PfEHD) associates with endocytosis and vesicular trafficking towards neutral lipid storage site. Biochim Biophys Acta - Mol Cell Res

1853:2856–2869.

34. Gueho A, Bosmani C, Gopaldass N, Molle V, Soldati T, Letourneur F. 2016. Dictyostelium EHD associates with Dynamin and participates in phagosome maturation. J Cell Sci 129:2354–2367.

35. Daumke O, Lundmark R, Vallis Y, Martens S, Butler PJG, McMahon HT. 2007. Architectural and mechanistic insights into an EHD ATPase involved in membrane remodelling. Nature 449:923–927.

36. Sharma M, Giridharan SSP, Rahajeng J, Naslavsky N, Aplan S. 2009. MICAL-L1 Links EHD1 to Tubular Recycling Endosomes and Regulates Receptor Recycling. Mol Biol Cell 20:4524–4530.

37. Pant S, Sharma M, Patel K, Caplan S, Carr CM, Grant BD. 2009. AMPH-1/Amphiphysin/Bin1 functions with RME-1/Ehd1 in endocytic recycling. Nat Cell Biol 11:1399–1410.

38. Lee DW, Zhao X, Scarselletta S, Schweinsberg PJ, Eisenberg E, Grant BD, Greene LE. 2005. ATP binding regulates oligomerization and endosome association of RME-1 family proteins. J Biol Chem 280:17213–17220.

39. Stoeber M, Stoeck IK, HéCurrency Signnni C, Bleck CKE, Balistreri G, Helenius A. 2012. Oligomers of the ATPase EHD2 confine caveolae to the plasma membrane through association with actin. EMBO J 31:2350–2364.

40. Deo R, Kushwah MS, Kamerkar SC, Kadam NY, Dar S, Babu K, Srivastava A, Pucadyil TJ. 2018. ATP-dependent membrane remodeling links EHD1 functions to endocytic recycling. Nat Commun 9.

41. Nakada-Tsukui K, Watanabe N, Maehama T, Nozaki T. 2019.

915 Phosphatidylinositol Kinases and Phosphatases in Entamoeba histolytica. Front
916 Cell Infect Microbiol 9:1–36.
917 42. Koushik AB, Powell RR, Temesvari LA. 2013. Localization of phosphatidylinositol
918 4,5-bisphosphate to lipid rafts and uroids in the human protozoan parasite
919 entamoeba histolytica. Infect Immun 81:2145–2155.
920 43. Swanson JA. 2014. Phosphoinositides and engulfment. Cell Microbiol 16:1473–
921 1483.
922 44. Wallroth A, Haucke V. 2018. Phosphoinositide conversion in endocytosis and the
923 endolysosomal system. J Biol Chem 293:1526–1535.
924 45. Odorizzi G, Babst M, Emr SD. 1998. Fab1p PtdIns(3)P 5-kinase function essential
925 for protein sorting in the multivesicular body. Cell 95:847–858.
926 46. Das K, Watanabe N, Nozaki T. 2021. Two StAR-related lipid transfer proteins play
927 specific roles in endocytosis, exocytosis, and motility in the parasitic protist
928 Entamoeba histolytica. PLoS Pathog 17:1–27.
929 47. Das A, Nag S, Mason AB, Barroso MM. 2016. Endosome-mitochondria
930 interactions are modulated by iron release from transferrin. J Cell Biol 214:831–
931 845.
932 48. Farmer T, Reinecke JB, Xie S, Bahl K, Naslavsky N, Caplan S. 2017. Control of
933 mitochondrial homeostasis by endocytic regulatory proteins. J Cell Sci 130:2359–
934 2370.
935 49. Wexler-Cohen Y, Stevens GC, Barnoy E, Van Der Bliek AM, Johnson PJ. 2014. A
936 dynamin-related protein contributes to Trichomonas vaginalis hydrogenosomal
937 fission. FASEB J 28:1113–1121.

938 50. Makiuchi T, Santos HJ, Tachibana H, Nozaki T. 2017. Hetero-oligomer of
939 dynamin-related proteins participates in the fission of highly divergent
940 mitochondria from Entamoeba histolytica. Sci Rep 7:1–13.
941 51. Santos HJ, Makiuchi T, Nozaki T. 2018. Reinventing an Organelle: The Reduced
942 Mitochondrion in Parasitic Protists. Trends Parasitol 34:1038–1055.
943 52. Soubannier V, McLelland GL, Zunino R, Braschi E, Rippstein P, Fon EA, McBride
944 HM. 2012. A vesicular transport pathway shuttles cargo from mitochondria to
945 lysosomes. Curr Biol 22:135–141.
946 53. Li Z, Schulze RJ, Weller SG, Krueger EW, Schott MB, Zhang X, Casey CA, Liu J,
947 Stöckli J, James DE, McNiven MA. 2016. A novel rab10-EHBP1-EHD2 complex
948 essential for the autophagic engulfment of lipid droplets. Sci Adv 2.
949 54. Diamond LS, Harlow DR, Cunnick CC. 1978. A new medium for the axenic
950 cultivation of Entamoeba histolytica and other Entamoeba. Trans R Soc Trop Med
951 Hyg1978/01/01. 72:431–432.
952 55. Bracha R, Nuchamowitz Y, Anbar M, Mirelman D. 2006. Transcriptional silencing
953 of multiple genes in trophozoites of Entamoeba histolytica. PLoS
954 Pathog2006/05/31. 2:e48.
955 56. Nakada-Tsukui K, Okada H, Mitra BN, Nozaki T. 2009. Phosphatidylinositol-
956 phosphates mediate cytoskeletal reorganization during phagocytosis via a unique
957 modular protein consisting of RhoGEF/DH and FYVE domains in the parasitic
958 protozoon Entamoeba histolytica. Cell Microbiol 11:1471–1491.
959 57. Mi-ichi F, Makiuchi T, Furukawa A, Sato D, Nozaki T. 2011. Sulfate activation in
960 mitosomes plays an important role in the proliferation of Entamoeba histolytica.

PLoS Negl Trop Dis 5:e1263.

58. Nozaki T, Asai T, Sanchez LB, Kobayashi S, Nakazawa M, Takeuchi T. 1999. Characterization of the Gene Encoding Serine Acetyltransferase , a Regulated Enzyme of Cysteine Biosynthesis from the Protist Parasites Entamoeba histolytica and Entamoeba dispar 274:32445–32452.

59. Chiba Y, Kamikawa R, Nakada-Tsukui K, Saito-Nakano Y, Nozaki T. 2015. Discovery of PPi-type Phosphoenolpyruvate Carboxykinase Genes in Eukaryotes and Bacteria. J Biochem 290:23960–23970.

60. Tomii K, Santos HJ, Nozaki T. 2019. Genome-wide analysis of known and potential tetraspanins in Entamoeba histolytica. Genes (Basel) 10:1–19.

61. Nozaki T, Asai T, Kobayashi S, Ikegami F, Noji M, Saito K, Takeuchi T. 1998. Molecular cloning and characterization of the genes encoding two isoforms of cysteine synthase in the enteric protozoan parasite Entamoeba histolytica. Mol Biochem Parasitol 97:33–44.

62. Nakada-Tsukui K, Tsuboi K, Furukawa A, Yamada Y, Nozaki T. 2012. A novel class of cysteine protease receptors that mediate lysosomal transport. Cell Microbiol 14:1299–1317.

63. Aurrecoechea C, Barreto A, Brestelli J, Brunk BP, Caler E V., Fischer S, Gajria B, Gao X, Gingle A, Grant G, Harb OS, Heiges M, Iodice J, Kissinger JC, Kraemer ET, Li W, Nayak V, Pennington C, Pinney DF, Pitts B, Roos DS, Srinivasamoorthy G, Stoeckert CJ, Treatman C, Wang H. 2011. AmoebaDB and MicrosporidiaDB: Functional genomic resources for Amoebozoa and Microsporidia species. Nucleic Acids Res 39:1–8.

64. Ludwiczak J, Winski A, Szczepaniak K, Alva V, Dunin-Horkawicz S. 2019. DeepCoil - A fast and accurate prediction of coiled-coil domains in protein sequences. Bioinformatics 35:2790–2795.

65. Nurkanto A, Jeelani G, Santos HJ, Rahmawati Y, Mori M, Nakamura Y, Goto K, Saikawa Y, Annoura T, Tozawa Y, Sakura T, Inaoka DK, Shiomi K, Nozaki T. 2021. Characterization of Plasmodium falciparum Pantothenate Kinase and Identification of Its Inhibitors From Natural Products. Front Cell Infect Microbiol 11:1–10.

66. Kumagai K, Kojima H, Okabe T, Nagano T. 2014. Development of a highly sensitive, high-throughput assay for glycosyltransferases using enzyme-coupled fluorescence detection. Anal Biochem 447:146–155.

67. Katoh K, Standley DM. 2013. MAFFT multiple sequence alignment software version 7: Improvements in performance and usability. Mol Biol Evol 30:772–780.

68. Waterhouse AM, Procter JB, Martin DMA, Clamp M, Barton GJ. 2009. Jalview Version 2-a multiple sequence alignment editor and analysis workbench. Bioinformatics 25:1189–1191.

Figure 1

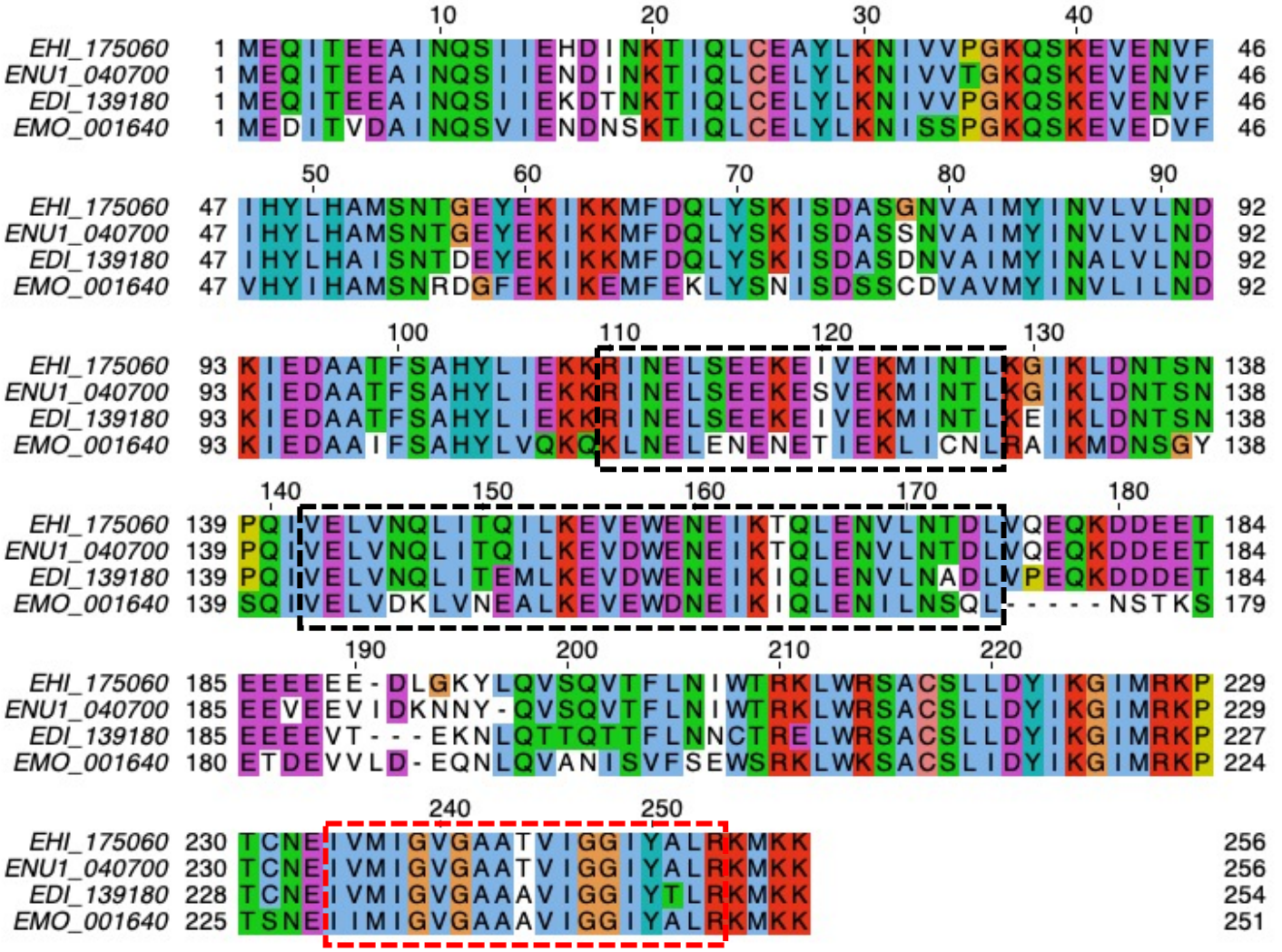
10
20
30
40
EHI_175060 1 MEQITEEAINQSIIEHDINKTIQLCEAYLKNIVVPGKQSKEVENVF 46
ENU1_040700 1 MEQITEEAINQSIIENDINKTIQLCELYLKNIVVTGKQSKEVENVF 46
EDI_139180 1 MEQITEEAINQSIIEKDTNKTIQLCELYLKNIVVPGKQSKEVENVF 46
EMO_001640 1 MEDITVDAINQSVIENDNSKTIQLCELYLKNISSPGKQSKEVEDVF 46
50
60
70
80
90
EHI_175060 47 IHYLHAMSNTGEYEKIKKMFDQLYSKISDASGNVAIMYINVLVLND 92
ENU1_040700 47 IHYLHAMSNTGEYEKIKKMFDQLYSKISDASSNVAIMYINVLVLND 92
EDI_139180 47 IHYLHAISNTDEYEKIKKMFDQLYSKISDASDNVAIMYINALVLND 92
EMO_001640 47 VHYIHAMSNRDGFEKIKEMFEKLYSNISDSSCDVAVMYINVLILND 92
100
110
120
130
EHI_175060 93 KIEDAATFSAHYLIEKKRINELSEEKEIVEKMINTLKGIKLDNTSN 138
ENU1_040700 93 KIEDAATFSAHYLIEKKRINELSEEKESVEKMINTLKGIKLDNTSN 138
EDI_139180 93 KIEDAATFSAHYLIEKKRINELSEEKEIVEKMINTLKEIKLDNTSN 138
EMO_001640 93 KIEDAAIFSAHYLVQKQKLNELENENETIEKLICNLRAIKMDNSGY 138
140
150
160
170
180
EHI_175060 139 PQIVELVNQLITQILKEVEWENEIKTQLENVLNTDLVQEQKDDEET 184
ENU1_040700 139 PQIVELVNQLITQILKEVDWENEIKTQLENVLNTDLVQEQKDDEET 184
EDI_139180 139 PQIVELVNQLITEMLKEVDWENEIKIQLENVLNADLVPEQKDDDET 184
EMO_001640 139 SQIVELVDKLVNEALKEVEWDNEIKIQLENILNSQL-----NSTKS 179
190
200
210
220
EHI_175060 185 EEEEEE-DLGKYLQVSQVTFLNIWTRKLWRSACSLLDYIKGIMRKP 229
ENU1_040700 185 EEVEEVIDKNNY-QVSQVTFLNIWTRKLWRSACSLLDYIKGIMRKP 229
EDI_139180 185 EEEEVT---EKNLQTTQTTFLNNCTREWRSACSLLDYIKGIMRKP 227
EMO_001640 180 ETDEVVLD-EQNLQVANISVFSEWSRKLWKSACSLIDYIKGIMRKP 224
240
250
EHI_175060 230 TCNEIVMIGVGAATVIGGIYALRKMKK 256
ENU1_040700 230 TCNEIVMIGVGAATVIGGIYALRKMKK 256
EDI_139180 228 TCNEIVMIGVGAAAVIGGIYTLRKMKK 254
EMO_001640 225 TSNEIIMIGVGAAAVIGGIYALRKMKK 251

Figure 2

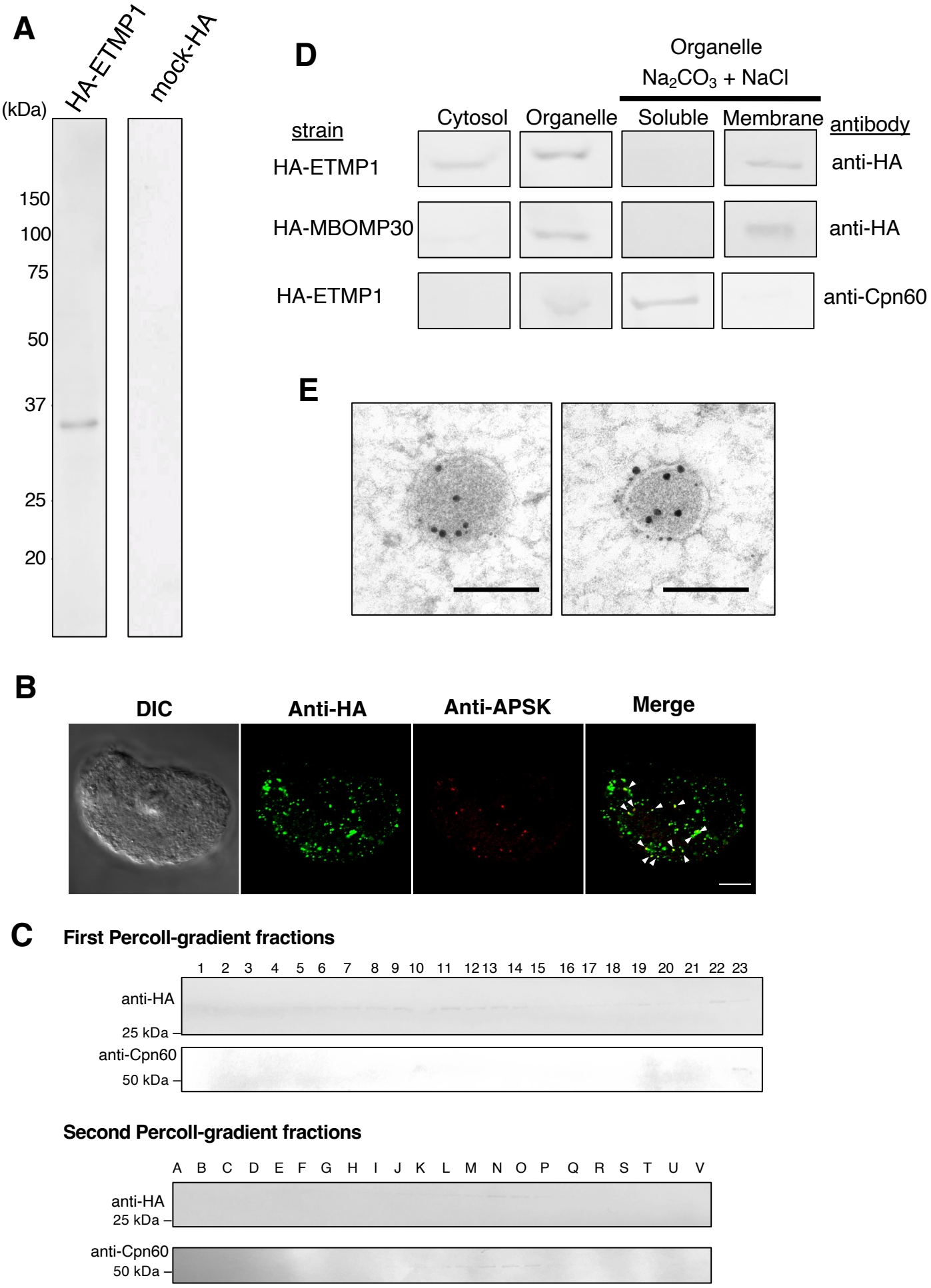
A
HA-ETMP1
mock-HA
(kDa)
150
100
75
50
37
25
20
D
Organelle
Na2CO3 + NaCl
Cytosol
Organelle
Soluble
Membrane
strain
antibody
HA-ETMP1
anti-HA
HA-MBOMP30
anti-HA
HA-ETMP1
anti-Cpn60
E
B
DIC
Anti-HA
Anti-APSK
Merge
C
First Percoll-gradient fractions
1 2 3 4 5 6 7 8 9 10 11 12 13 14 15 16 17 18 19 20 21 22 23
anti-HA
25 kDa
anti-Cpn60
50 kDa
Second Percoll-gradient fractions
A B C D E F G H I J K L M N O P Q R S T U V
anti-HA
25 kDa
anti-Cpn60
50 kDa

Figure 3

A

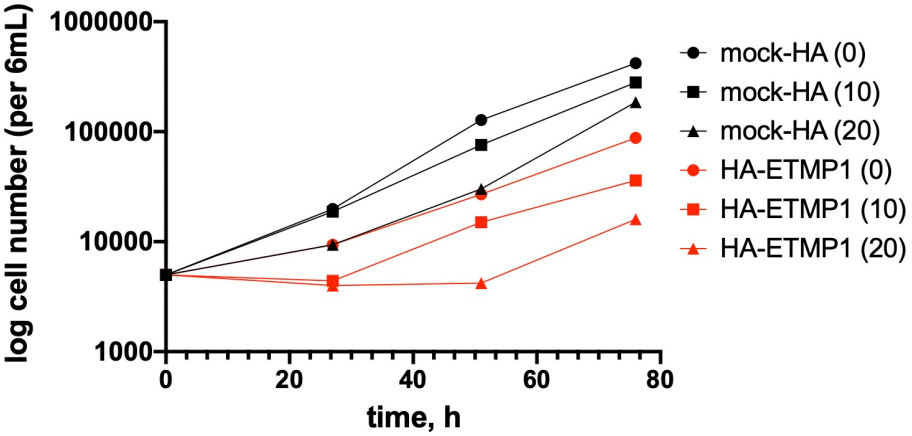
log cell number (per 6mL)
1000000
100000
10000
1000
0
20
40
60
80
time, h
mock-HA (0)
mock-HA (10)
mock-HA (20)
HA-ETMP1 (0)
HA-ETMP1 (10)
HA-ETMP1 (20)

B

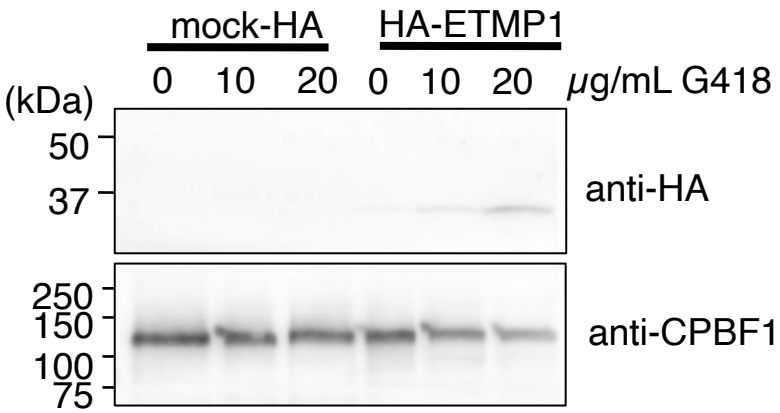
mock-HA
HA-ETMP1
0 10 20 0 10 20 μg/mL G418
(kDa)
50
37
anti-HA
250
150
100
75
anti-CPBF1

Figure 4

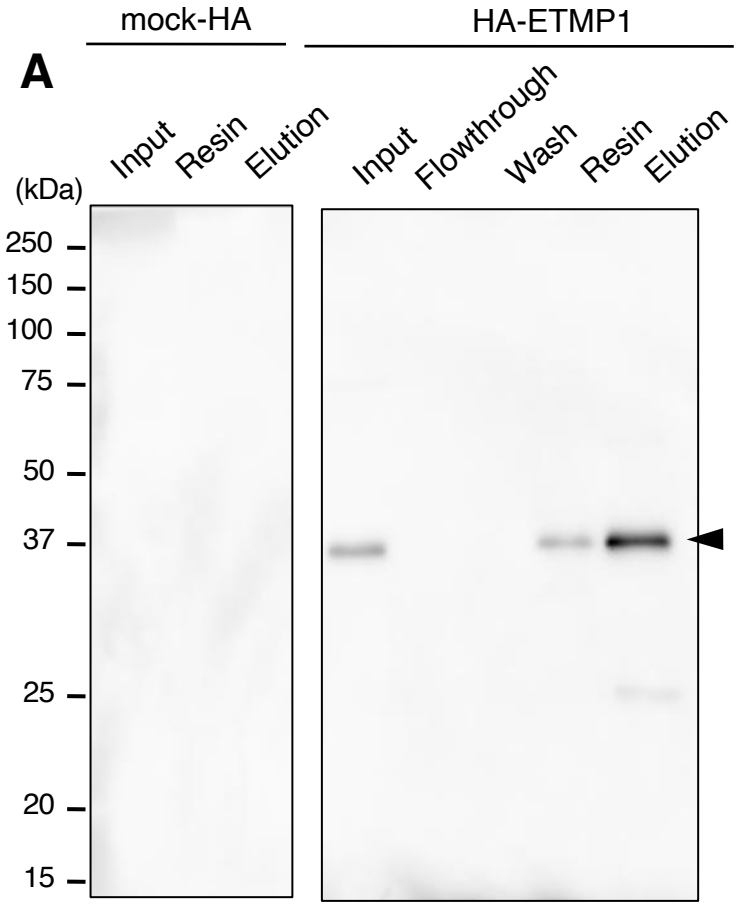

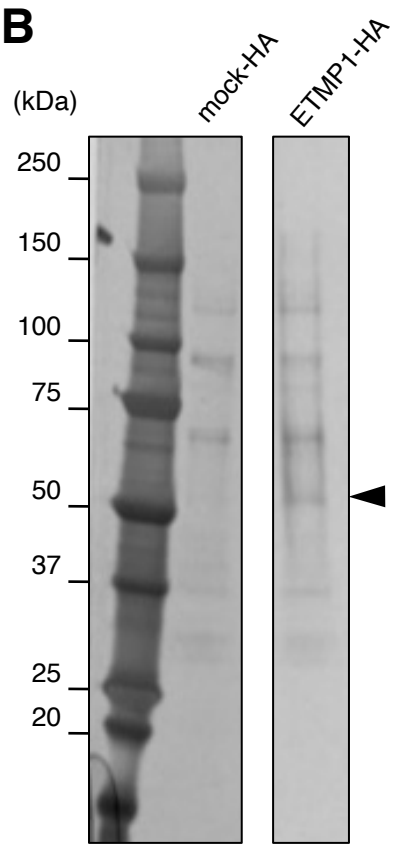

C

Protein Name	Accession Number	MW (kDa)	Qv HA-ETMP1	Qv mock-HA	Mitosome proteome
L-myo-inositol-1-phosphate synthase	EHI_070720	57	9	2	+
Vacuolar protein sorting-associated protein 45	EHI_154290	60	4	0	-
EH-domain containing protein (EHD1)	EHI_105270	58	2	0	+
EH-domain containing protein (EHD2)	EHI_152680	58	2	0	+

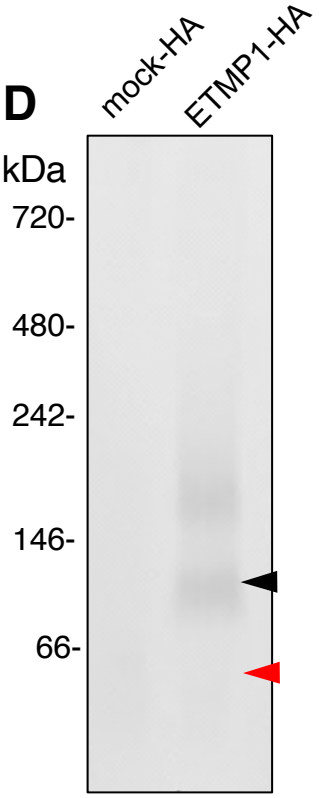

Figure 5

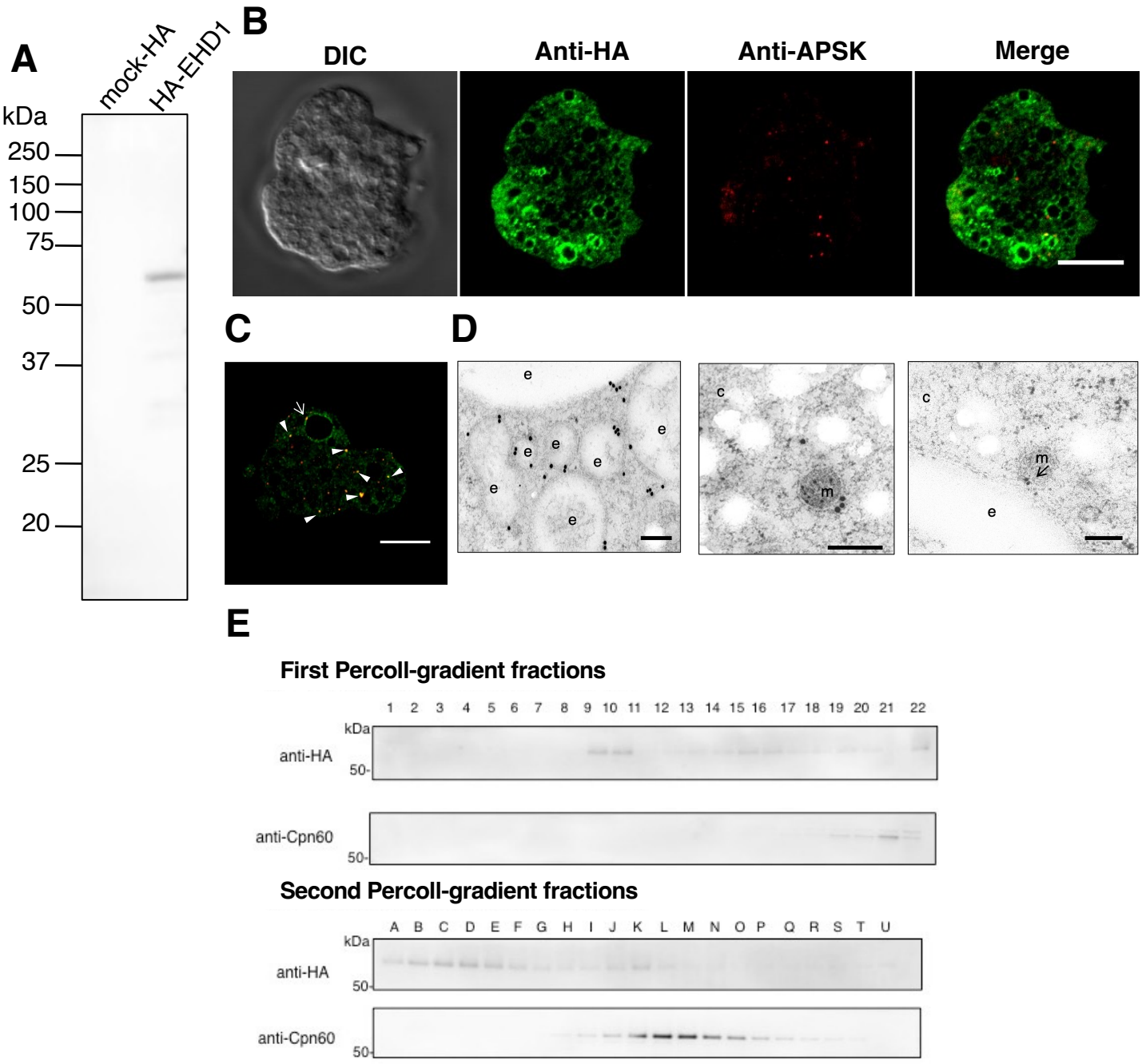
A
mock-HA
HA-EHD1
kDa
250
150
100
75
50
37
25
20
B
DIC
Anti-HA
Anti-APSK
Merge
C
D
e
c
m
E
First Percoll-gradient fractions
1 2 3 4 5 6 7 8 9 10 11 12 13 14 15 16 17 18 19 20 21 22
kDa
anti-HA
50-
anti-Cpn60
50-
Second Percoll-gradient fractions
A B C D E F G H I J K L M N O P Q R S T U
kDa
anti-HA
50
anti-Cpn60
50

Figure 6

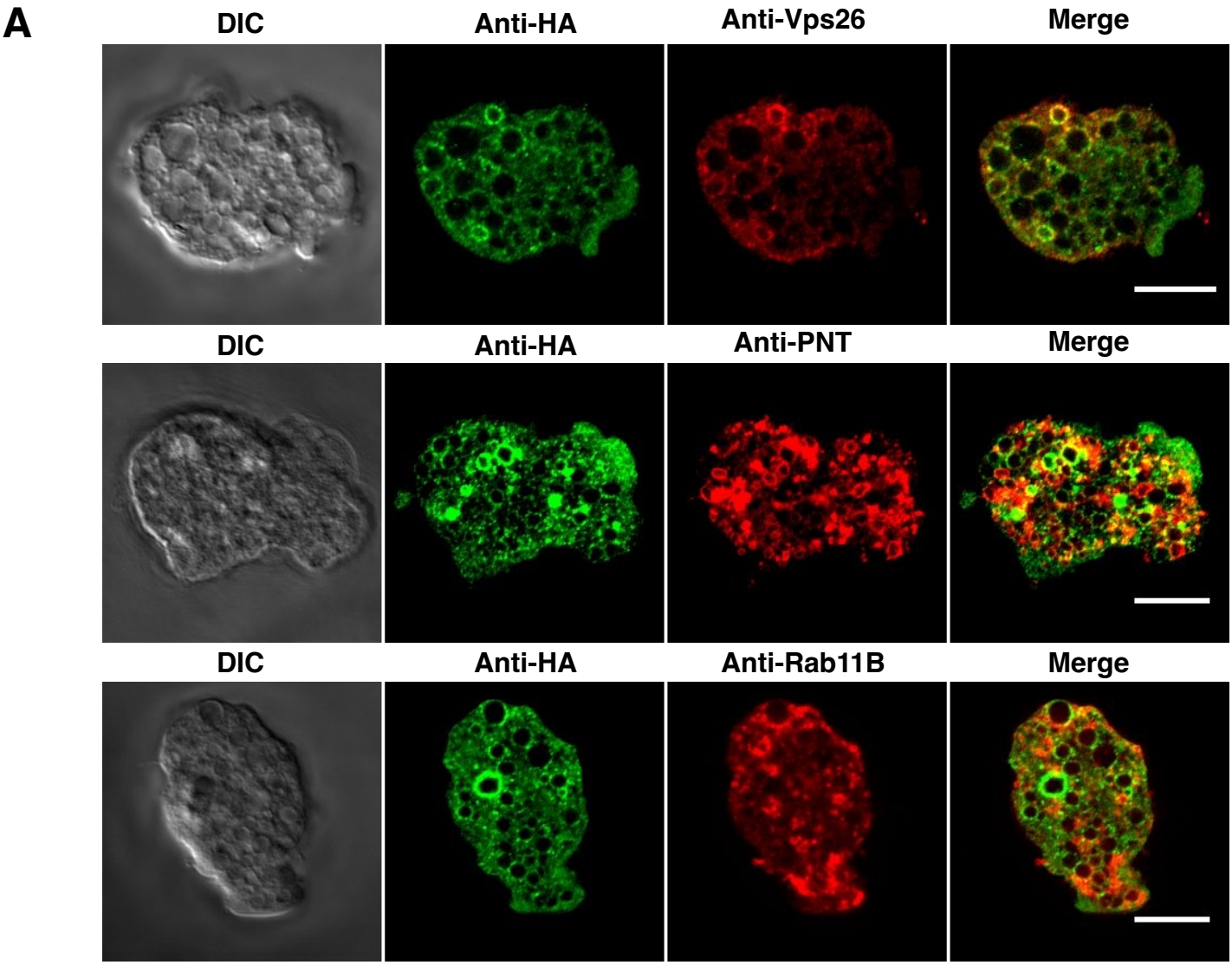
A
DIC
Anti-HA
Anti-Vps26
Merge
DIC
Anti-HA
Anti-PNT
Merge
DIC
Anti-HA
Anti-Rab11B
Merge

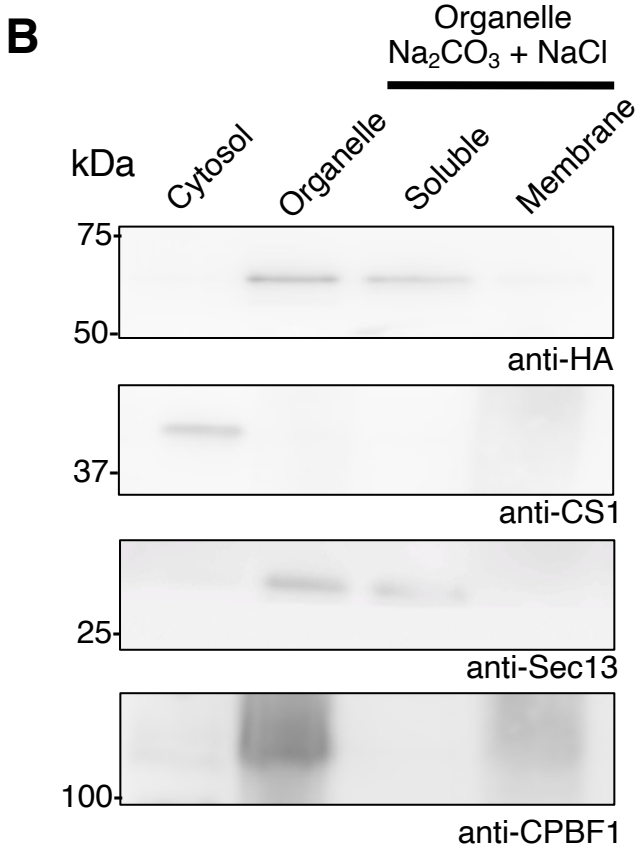
B
Organelle
Na2CO3 + NaCl
kDa
Cytosol
Organelle
Soluble
Membrane
75
50
anti-HA
37
anti-CS1
25
anti-Sec13
100
anti-CPBF1

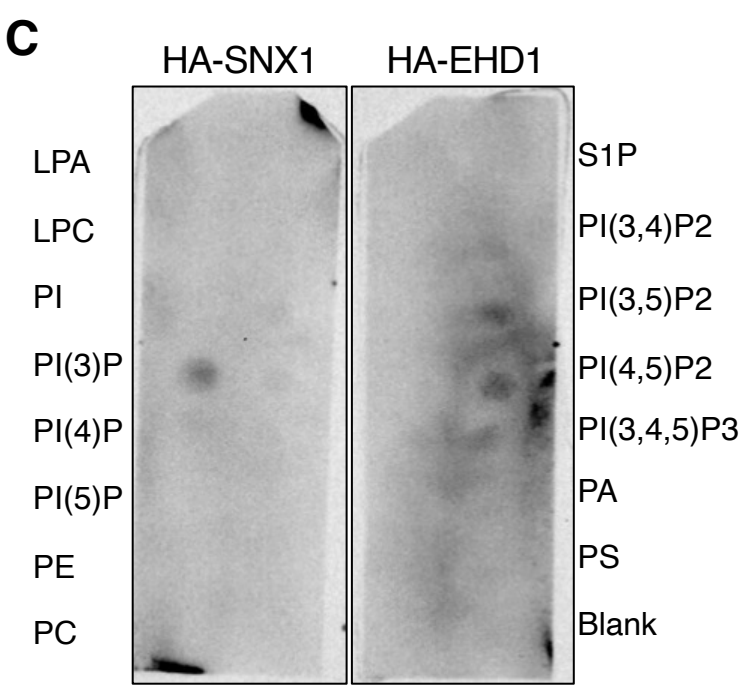
C
HA-SNX1
HA-EHD1
LPA
LPC
PI
PI(3)P
PI(4)P
PI(5)P
PE
PC
S1P
PI(3,4)P2
PI(3,5)P2
PI(4,5)P2
PI(3,4,5)P3
PA
PS
Blank

Figure 7

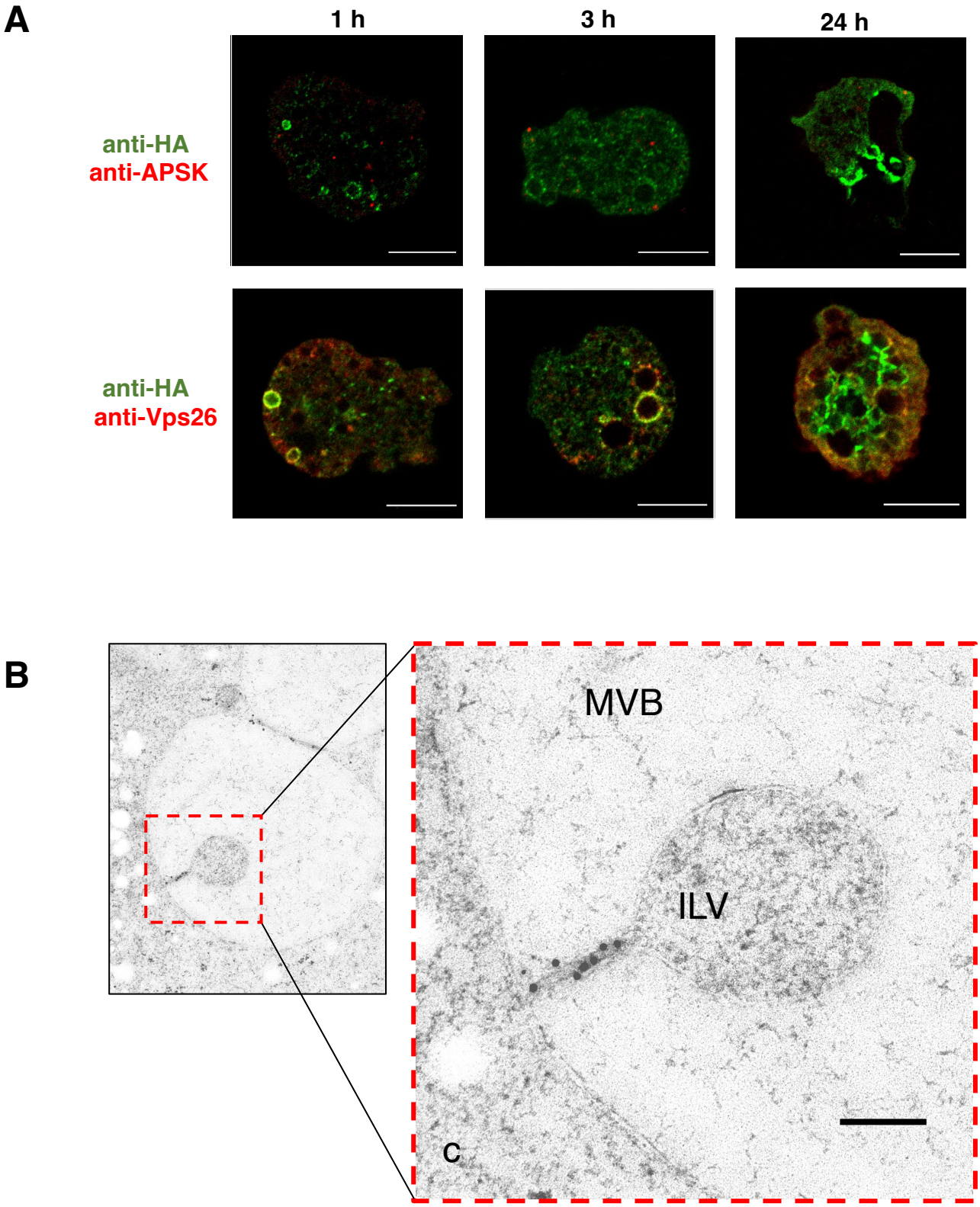

Figure 8

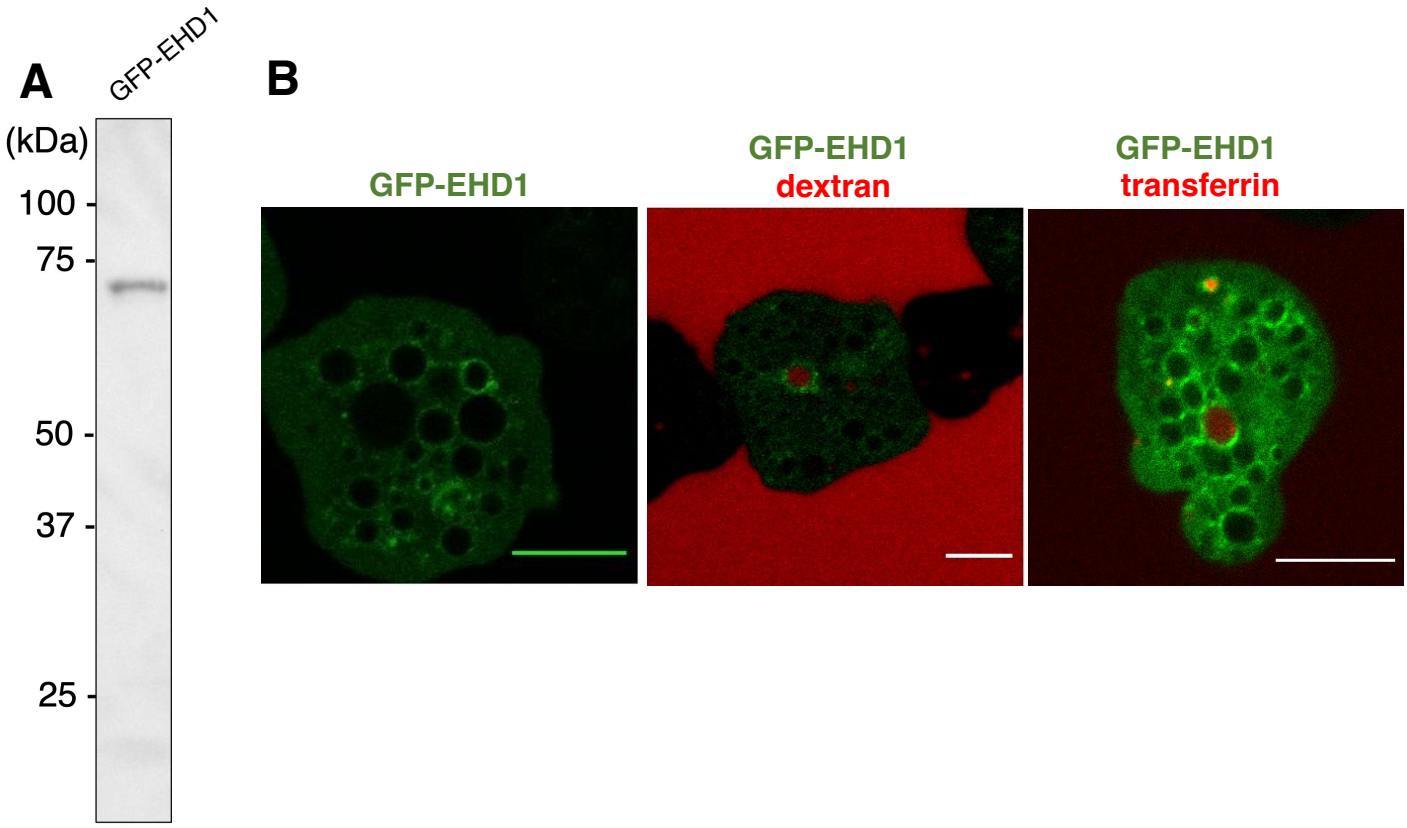
A
GFP-EHD1
(kDa)
100
75
50
37
25
B
GFP-EHD1
GFP-EHD1
dextran
GFP-EHD1
transferrin

Figure 9

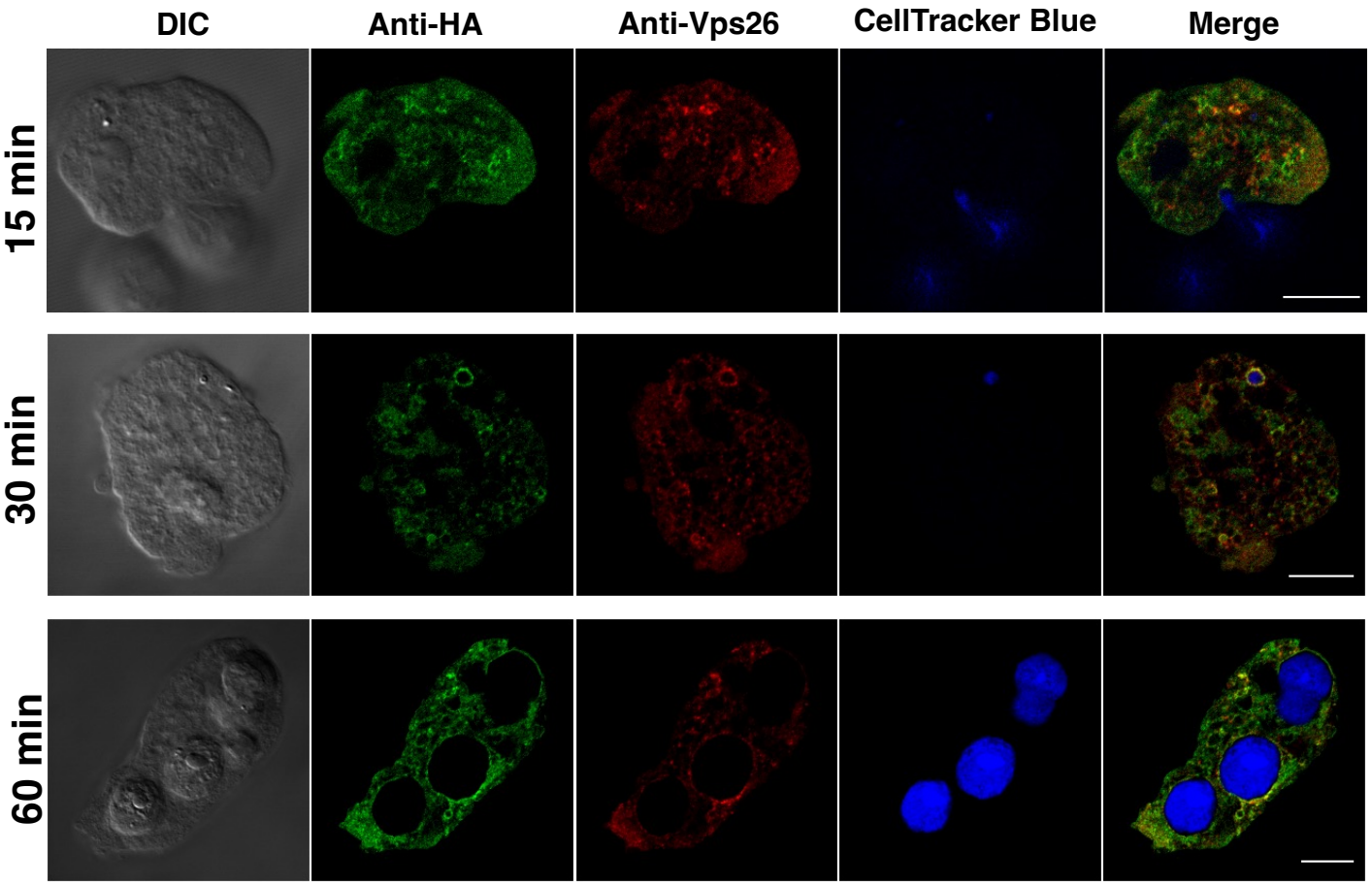
DIC
Anti-HA
Anti-Vps26
CellTracker Blue
Merge
15 min
30 min
60 min

Figure 10

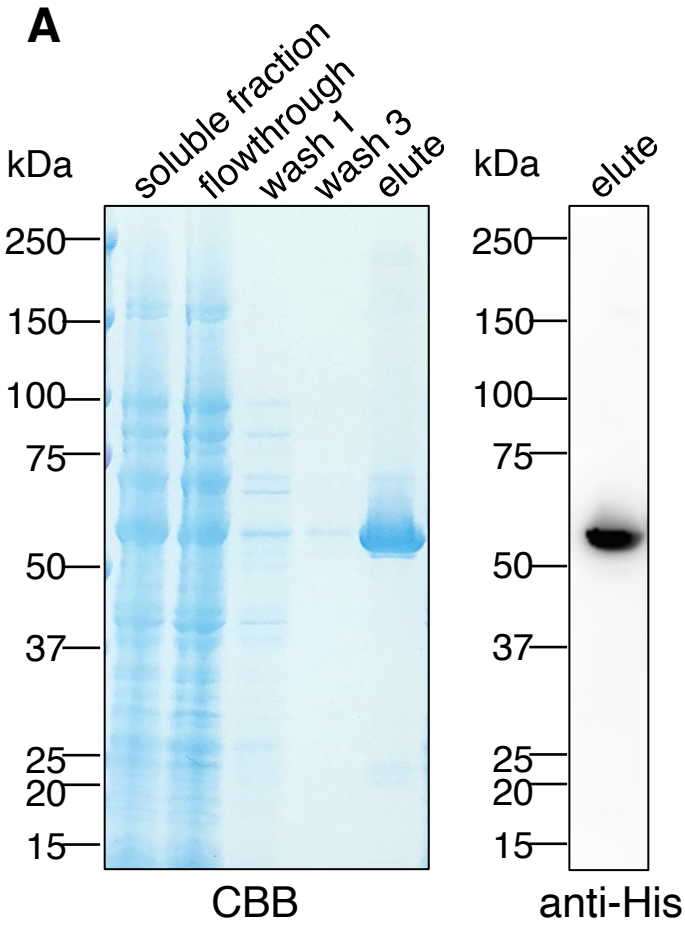
A
soluble fraction
flowthrough
wash 1
wash 3
elute
kDa
250
150
100
75
50
37
25
20
15
CBB
kDa
elute
250
150
100
75
50
37
25
20
15
anti-His

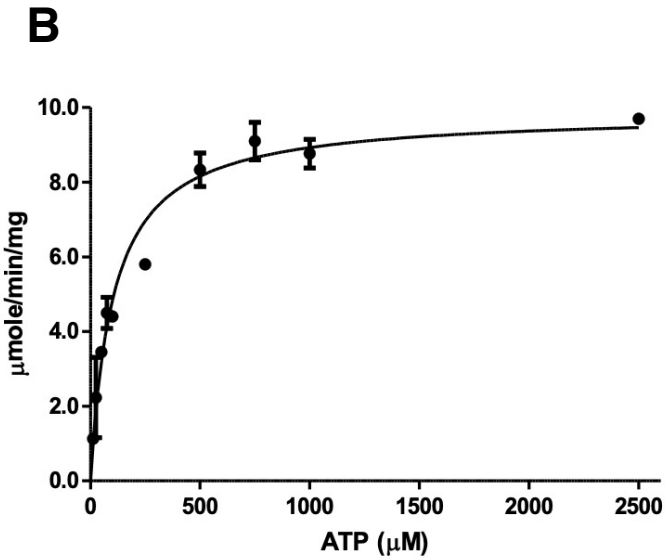
B
μmole/min/mg
10.0
8.0
6.0
4.0
2.0
0.0
0
500
1000
1500
2000
2500
ATP (μM)